International Journal of Quantum Chemistry

WILEY

International Journal of QUANTUM CHEMISTRY

RESEARCH ARTICLE OPEN ACCESS

Investigation of Hydantoin-Based Drugs Used in the Treatment of Epilepsy Using Quantum Chemical Calculations, Molecular Docking, Molecular Dynamics, ADMET, In Vitro, and Spectroscopic Methods

Minnet Can Kandemir[1,2] | Bilge Bicak[2] | Serda Kecel-Gunduz[2] | Gizem Akman[3]

[1]Department of Physics, Freie Universität Berlin, Berlin, Germany | [2]Department of Physics, Science Faculty, Istanbul University, Istanbul, Turkey | [3]Department of Biology, Science Faculty, Istanbul University, Istanbul, Turkey

Correspondence: Serda Kecel-Gunduz (skecel@istanbul.edu.tr)

Received: 2 January 2024 | **Revised:** 21 May 2024 | **Accepted:** 3 September 2024

Funding: This work was supported by Türkiye Bilimsel ve Teknolojik Araştırma Kurumu and Bilimsel Araştirma Projeleri Birimi, Istanbul Üniversitesi.

Keywords: ADMET | hydantoin-based drug | molecular docking | molecular dynamics | spectroscopy

ABSTRACT

Present investigation deals with the structural and pharmacokinetic properties of hydantoin-based drug molecules such as phenytoin, mephenytoin, and ethotoin. Hydantoin-based drugs are widely used as anticonvulsants in the treatment of epilepsy. In this study, optimized structures, and theoretical vibrational wavenumbers of phenytoin, mephenytoin, and ethotoin molecules were determined using Gaussian 09 program with density functional theory (DFT) and B3LYP/6-311++G(d,p) basis set, vibration mode assignments were performed with the GAR2PED program, and the theoretical results were supported by FTIR and Raman spectroscopy. In addition, thermodynamic parameters, Mulliken charge values, HOMO-LUMO, natural bond orbital, MEP, hyperpolarizability analyzes of hydantoin-based molecules were performed. Docking analysis of all molecules with the GABA-AT receptor, which has an important place in epilepsy studies, were also carried out. Then, the molecular dynamic (MD) simulations of the hydantoin-based drugs-GABA-AT complexes were realized for 50 ns. ADMET profiles of all molecules were determined and presented by parameters of toxicity and drug-likeness. Additionally, to determine the effects of hydantoin-based drugs on glioblastoma cells, cytotoxic effects of phenytoin, mephenytoin, and ethotoin were evaluated on U-87 Human glioblastoma cell line.

1 | Introduction

Epilepsy, one of the most common central nervous system (CNS) diseases, is a nervous disorder caused by an abnormal electro-chemical discharge of nerve cells in the brain. The causes of epilepsy are classified as structural, genetic, infectious, metabolic, immune, and unknown. People with epilepsy often have recurrent seizures, spontaneously, and without any symptoms [1, 2]. Seizure onsets are classified as focal (occurring in one hemisphere of the brain), generalized (occurring in both hemispheres simultaneously), and unknown onset. Appropriate treatment can be selected by classifying the seizure types [2]. In the treatment of epilepsy, factors such as seizure type and age of the patient are evaluated separately, and treatment is started. Most people with epilepsy use drugs that do not affect their quality of life and are effective in stopping seizures [3].

Antiepileptic (Anticonvulsant) drugs aim to eliminate or reduce the seizures, avoid side effects caused by long-term treatment, and enable people to sustain a normal life [4]. In the treatment of epilepsy, antiepileptic drugs are used as pharmacological agents in the treatment of epileptic seizures. When a seizure occurs, antiepileptic drugs aim to prevent neurons from discharging excessively and spreading the seizure into the brain [5, 6].

Modulation of voltage-gated ion channels and increase of GABA-mediated inhibitory neurotransmission are important in the mechanisms of action of antiepileptic drugs [7]. Gamma-aminobutyric acid (GABA) is an inhibitory neurotransmitter responsible for regulating various neurological functions of CNS pathways. GABA-AT is an important target for antiepileptic drugs. GABA-AT has selective inhibition and thus, raises GABA concentrations in brain [8]. Consuming of GABA causes convulsions and thus, inhibition of GABA-AT can be therapeutic in epilepsy studies [9]. Hydantoin-based phenytoin, whose trade name is dilantin, is widely used as an antiepileptic drug and plays important roles such as GABAergic neurotransmission [10] and sodium channel blockade [11]. In studies with phenytoin and GABA, it was reported that phenytoin increases the effect of GABA [10]. It was reported that low-dose phenytoin may play a role in increasing GABA neurotransmission and, accordingly, in maintaining the balance between the GABAergic and glutaminergic systems [12]. Mephenytoin (Mesantoin) and ethotoin (Peganone) were also used as anticonvulsants [13]. Mephenytoin and ethotoin were used in the 1940s and 1950s. In the literature, it was reported that mephenytoin is more effective than ethotoin [13]. Nonetheless, among the hydantoin-based drugs such as etotoin, mephenytoin, and phenytoin was the most studied and used is the phenytoin. The other hydantoin-based drugs such as ethotoin and mephenytoin were less used because of a higher percentage of unfavorable reactions or lower effect [10]. Glioblastoma is a lethal and invasive tumor, and neuronal mechanisms can trigger the growth and distribution of Glioblastoma cells. Glioblastoma cells and changes in peritumoral tissues may cause epileptic symptoms in patients with Glioblastoma tumors through common signals mediated by neurotransmitters such as GABA and glutamate. It has been reported that some drugs used in the treatment of epilepsy may be effective in the treatment of cancer when used as local treatment [14–16].

In this study, structural analyzes of hydantoin-based drugs ethotoin, mephenytoin, and phenytoin were carried out theoretically and experimentally. First, optimized geometries, vibrational wave numbers, HOMO-LUMO, natural bond orbital, MEP, hyperpolarizability, thermodynamics, mulliken atomic charge calculations of drug molecules were performed with DFT/B3LYP/6311++G(d,p). Then, infrared (IR) and Raman spectra of the molecules were obtained, and experimental and theoretical wavenumbers were compared and presented with the potential energy distributions. Molecular docking studies were carried out with the GABA-AT receptor, which is an important pharmacological target of drugs. As a result of molecular docking calculations performed, the interaction sites, and binding affinities of the drugs with the receptor were determined. The molecular dynamic (MD) simulations of the hydantoin-based drugs-GABA-AT complexes were carried out. In addition, ADMET profiles of drugs were also calculated. In addition, to clarify the anti-tumor efficacy of some hydantoin-based epilepsy drugs based on glioblastoma-specific biomarkers, cytotoxicity studies were performed on the glioblastoma cell line.

2 | Material and Methods

2.1 | Materials

Phenytoin ($C_{15}H_{12}N_2O_2$, Cas No: 57-41-0), Mephenytoin ($C_{12}H_{14}N_2O_2$, Cas No: 70989-04-7) and Ethotoin ($C_{11}H_{12}N_2O_2$, Cas No: 86-35-1) were purchased from Cayman Chemical.

2.2 | Methods

2.2.1 | Structural Analysis

Geometric structures of Phenytoin (ZINC2510358), Mephenytoin (ZINC453), Ethotoin (ZINC271) molecules were taken from ZINC Database. Molecules were fist optimized at Gaussian 09 package program using DFT (B3LYP) method and 6-311++G(d,p) basis set and obtained the theoretical vibrational wavenumbers. In addition, the Mulliken charges and thermodynamic parameters of hydantoin-based molecules were obtained using the DFT/B3LYP/6-311++G(d,p) basis set.

2.2.2 | FTIR, Raman and PED Analyses

The theoretical wavenumbers were firstly scaled [17], and the vibration modes were assigned with the percentage contributions of each vibrational wavenumber using the Gar2PED program [18]. IR spectra using the KBr disk technique of hydantoin-based molecules were recorded on a Jasco300E FT-IR Spectrometer with $4000-400\,cm^{-1}$ spectral region with $2\,cm^{-1}$ resolutions. The micro-Raman spectra of hydantoin-based molecules were recorded at room temperature under 20× Olympus objective microscope on a Jasco NRS-3100 micro-Raman spectrometer. To filter the Rayleigh scattering, one notch filter was used. Using the silicon phonon mode at $520\,cm^{-1}$, the calibration of the spectrometer was provided. The Raman spectra of the hydantoin-based molecules were obtained with a Jasco NRS-3100 micro-Raman spectrometer (1200 lines/mm grating and high sensitivity cooled CCD).

2.2.3 | Molecular Electrostatic Potential Analysis

Molecular electrostatic potential maps can be used for getting information about hydrogen bond regions and structural activity [19]. Molecular electrostatic potential (MEP) maps illustrate electrophilic and nucleophilic regions. MEP surface defined by different colors from red to blue. The red color indicates the relative abundance of electrons, that is, the lowest electrostatic potential energy regions, which defines the electrophilic regions. The blue color indicates the relative absence of electrons, that is, the highest electrostatic potential energy regions, which defines the nucleofilic regions. Electrostatic potential values are lined up energetically as red < orange < yellow < green < blue [20, 21]. The MEP analyses for hydantoin-based drug molecules were performed at

Gaussian09 package program using DFT/B3LYP/6-311++G(d,p) basis set.

2.2.4 | HOMO-LUMO

Using DFT method, B3LYP theory level and 6-311++G(d,p) basis set, HOMOs, LUMOs, and HOMO-LUMO gaps (ΔE) of the hydantoin-based drug molecules were calculated at Gaussian 09 package program. In addition, the ionization potential (I), the electron affinity (A), the absolute electronegativity (χ), chemical potential (μ), and the chemical hardness (η) values were obtained for hydantoin-based drug molecules such as phenytoin, mephenytoin, and ethotoin.

2.2.5 | Natural Bond Orbital Analysis

In computational studies, localized (natural) orbitals are used to calculate the distribution of electron density in atoms and bonds between atoms [22]. NBO analysis is performed by examining all possible interactions between donor (filled) Lewis-type NBOs and acceptor (empty) non-Lewis-type NBOs and estimating their energetic significance with second-order perturbation theory [23, 24]. NBO analyses of hydantoin-based drug molecules were carried out at Gaussian 09 package program with the DFT/B3LYP/6-311++G(d,p) basis set.

For each donor, NBO (i) and acceptor NBO (j), the stabilization energy E (2) associated with the i-j delocalization is given as follows.

$$E(2) = \Delta E_{ij} = q_i \frac{F(i,j)^2}{\varepsilon_j - \varepsilon_i} \quad (1)$$

Here, q_i defines donor orbital occupancy, diagonal elements ε_i and ε_j orbital energies and $F(i,j)$ non-diagonal NBO Fock matrix element.

2.2.6 | Molecular Docking and ADMET Analyses

GABA is an important inhibitory neurotransmitter with vital neurological roles in the brain, while γ-aminobutyric acid aminotransferase (GABA-AT) is involved in the brain as a pyridoxal 5′-phosphate (PLP)-dependent enzyme that breaks down γ-aminobutyric (GABA). Therefore, GABA-AT has become an important drug target that regulates GABA level. Gamma-aminobutyric acid aminotransferase (PDB ID: 4Y0D) was selected as receptors [25]. For molecular docking and MD analysis, the Schrodinger Maestro version 11.4 software [26–28] was chosen and Phenytoin, Mephenytoin, Ethotoin molecules were prepared after the optimization process as ligands structures. Using the LigPrep module, possible poses belonging to all ligands were determined. The structure of 4-aminobutyrate aminotransferase with 2.19 Å resolution, which formed A,B,C,D, chains containing 463 sequence length having ligands, Fe2S2 inorganic cluster, and glycerol was extracted from the protein database. The homo2mer structure of this receptor was downloaded from the Swiss model [29] and adjusted so that only the A chain remained from the A and B chains. While the Fe2S2 inorganic cluster located near the natural ligand was kept, all water and ions that were not in the binding site of the natural ligand were deleted. The receptor structure was optimized with the protein preparation tool using the OPLS3 force field [30] and made ready for docking analysis. After creating a 3D grid box that placed the center of gravity of each ligand at its center and identifying all residues containing thiol and hydroxyl groups in the binding region of the receptor, each ligand was docked to the receptor, and its binding affinities and binding sites were evaluated.

Pharmacokinetic and toxicity profiles (ADMET properties) of Phenytoin, Mephenytoin, Ethotoin were determined by SwissADME [31] and PreADMET [32] online servers.

2.2.7 | MD Analysis

The stabilities of Phenytoin, Mephenytoin, Ethotoin molecules complex with 4-aminobutyrate aminotransferase (PDB ID: 4Y0D) were analyzed using the Desmond simulation package of the Schrödinger program with the OPLS force field [26, 30, 33]. All complexes were adjusted with a minimum distance of 10 Å between complex atoms and the box edges. All complexes were solvated by adding TIP3P water molecules [34, 35]. The system containing the complex was neutralized by adding counter ions Na^+ and Cl^-. Before simulation step, the energy minimization step was carried out using the Steepest Descent gradient algorithm. The isothermal and isobaric conditions of the system were adjusted to 300 K and 1 bar using the Nose–Hoover chain thermostat [36] and Martyna–Tobias–Klein barostat methods [37], respectively. After all preparation steps were carried out, MD simulations of all systems were performed for 50 ns. RMSDs of protein–ligand complexes, protein RMSF, and the information of protein–ligand complex contacts and interactions were obtained, after the simulations were completed.

2.2.8 | In Vitro Studies

Human glioblastoma cell line U-87 was used for in vitro cytotoxicity assays. U-87 cells were maintained in DMEM (Gibco) medium containing 10% of FBS (Gibco) and 1% Penicilin/Streptomycin (Gibco). U-87 cells incubated in 37°C and 5% CO_2. For MTT assay, U-87 cells were seeded at a density of 5×10^3 per well and incubated for 24 h in 96-well culture plate. After incubation period, medium was replaced with medium containing 100, 200, and 400 μM of Phenytoin/Ethotoin/Mephenytoin. At the end of 24 h experimental period, 40 μL MTT (Sigma) was added to the each well to form formazan crystals. Then, cells were incubated for 4 h at 37°C. A volume of 160 μL DMSO (Merck) added to wells as a solvent and incubated overnight. The measurement was performed using Elisa Reader at 570 nm (BioTek, ELx800). The results are expressed relative to the control value. The experiment was repeated three times independently.

2.2.9 | Statistical Analysis

One-way ANOVA was used to determine the significance of in vitro cytotoxic experiments followed by post hoc Dunnett's multiple comparison. $p < 0.05$ was considered as statistically significant. All calculations were performed using GraphPad Prism software (Version 6.0, GraphPad Software Inc., USA).

3 | Results and Discussion

3.1 | Geometrical Parameters

Optimized geometries of hydantoin-based molecules were determined and obtained bond, angle and dihedral values of these geometries at Gaussian 09 package program [38] with DFT (B3LYP) theory level and 6-311++G(d,p) basis set (see Figure 1, Table 1, Tables S1–S6). Phenytoin, one of the hydantoin-based drugs, has 31 atoms and has a vibrational wave number of 87. Mephenytoin, has 30 atoms and 84 vibrational wave numbers. Ethotoin has 27 atoms and 75 vibrational wave numbers. Additionally, the fundamental vibrational wave numbers of the molecules were calculated and the potential energy distribution (%PED) was used to analyze the vibrational modes.

When the bond and angle values of the molecules were compared with the literature, the NH bond length of phenytoin in the hydantoin ring were determined as 1.009 Å (theoretical result) [39]. In our study, the bond length was calculated as 1.0088 Å, similar to the literature values. When focusing on the hydantoin ring, it was seen that the bond and angle values of crystal structure in the literature were similar to the theoretical values in this study [40]. CO, CN, CC, NH bond lengths in the hydantoin rings of phenytoin, mephenytoin, and ethotoin were calculated and obtained values were found to be compatible with the literature (see Table 1) [40, 41]. N13-C7 bond length of hydantoin ring in

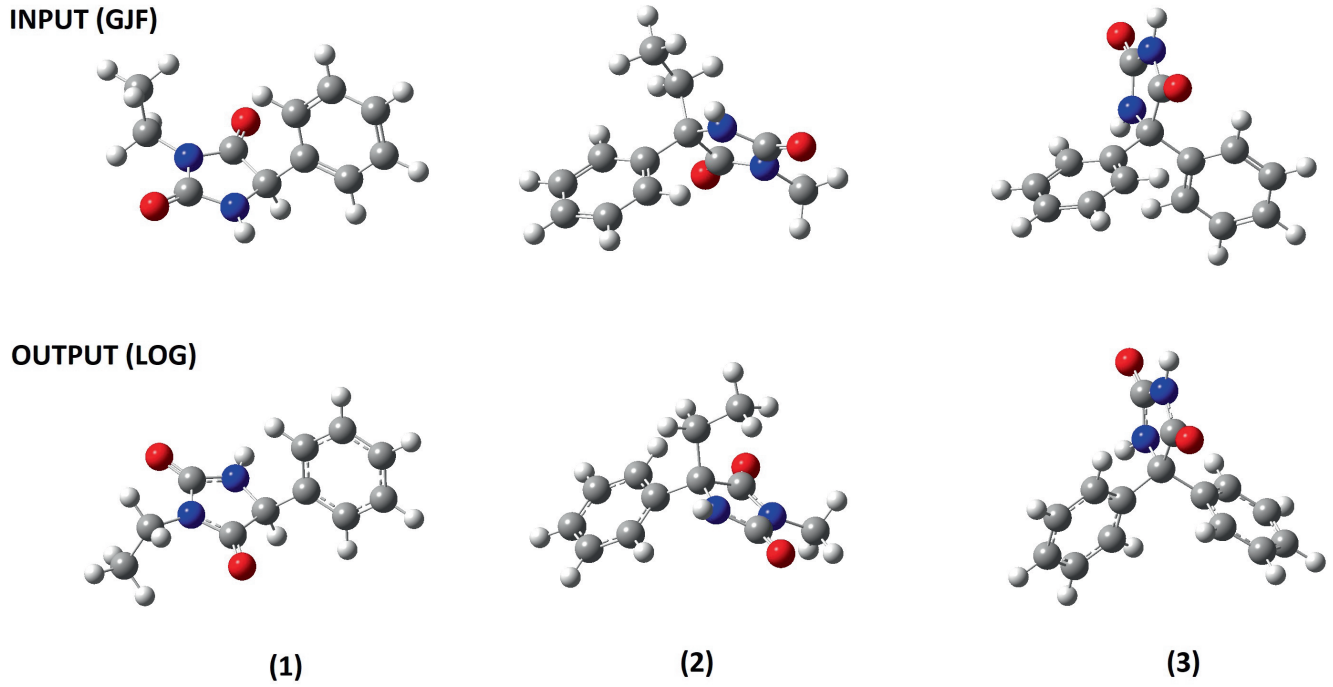

FIGURE 1 | The molecular structure of the ethotoin (1), mephenytoin (2), phenytoin (3) molecules.

TABLE 1 | Parameters of the hydantoin ring.

Phenytoin	Mephenytoin	Ethotoin	References
C7-N13: **1.471**	C3-N9: **1.460**	C6-N8: **1.452**	1.473 [41], 1.46 [40]
N13-C11: **1.371**	N9-C7: **1.367**	N8-C9: **1.369**	1.382 [41], 1.333 [40]
C11-O12: **1.208**	C7-O8: **1.210**	C9-O10: **1.210**	1.241 [41], 1.209 [40]
N13-H26: **1.009**	N9-H22: **1.008**	N8-H22: **1.007**	1.010 [41]
C11-N10: **1.408**	C7-N6: **1.413**	C9-N3: **1.413**	1.423 [41], 1.392 [40]
N10-C8: **1.374**	N6-C4: **1.374**	N3-C4: **1.377**	1.387 [41], 1.343 [40]
C7-C8: **1.562**	C4-C3: **1.552**	C4-C6: **1.549**	1.56 [41], 1.548 [40]
C8-O9: **1.205**	C4-O5: **1.210**	C4-O5: **1.210**	1.241 [41], 1.223 [40]
C7-C8-N10: **106.033**	C3-C4-N6: **107.166**	C6-C4-N3: **106.571**	110.34 [41], 107.3 [40]
C7-C8-O9: **127.061**	C3-C4-O5: **126.677**	C6-C4-O5: **126.565**	126.36 [41], 125.6 [40]
C8-N10-C11: **113.663**	C4-N6-C7: **112.099**	C4-N3-C9: **112.246**	113.24 [41], 112.6 [40]
N10-C11-N13: **105.549**	N6-C7-N9: **106.153**	N3-C9-N8: **106.296**	105.41 [41], 106.6 [40]
C7-N13-C11: **113.809**	C3-N9-C7: **114.01**	C6-N8-C9: **113.556**	114.18 [41], 114.2 [40]
C7-N13-H26: **121.775**	C3-N9-H22: **124.079**	C6-N8-H22: **124.688**	124.33 [41]

the phenytoin were calculated 1.47 Å, while it was determined as 1.46 and 1.47 Å in the literature. Similarly, it was observed that the bond lengths of the same NH groups in the hydantoin rings of mephenytoin and ethotoin were 1.46 and 1.45 Å, and these values were consistent with the literature values (see Table 1). Additionally, the bond lengths at the point where the hydantoin ring is attached to the other rings were calculated as 1.535 Å (phenytoin), 1.536 Å (mephenytoin), and 1.519 Å (ethotoin) in this study and were found as 1.531 Å in the literature [40]. In addition, it was determined that the angles in the hydantoin rings is attached to other rings are in full agreement with the literature [40]. Moreover, it was seen that the angles in the hydantoin ring were consistent with the literature values [40, 41]. Considering all these data, it was determined that the optimized geometric structures of phenytoin, mephenytoin, and ethotoin were similar to the theoretical and experimental values in the literature.

3.2 | PED Analysis

The fundamental vibrational wavenumbers of Phenytoin, Mephenytoin, and Ethotoin obtained experimentally with FT-IR and Raman spectroscopies and theoretically with Gaussian 09 program using DFT-B3LYP/6311++G(d,p) basis set. In this study, the theoretical wavenumbers were scaled using scale factors, first. Scale factors for B3LYP/6-311++G(d,p) basis set were chosen as 0.958 for above 1800 cm^{-1} and 0.983 for below 1800 cm^{-1} [17]. The assignments of the vibrational wavenumbers and the obtained experimental wavenumbers using FT-IR and Raman spectra of Phenytoin, Mephenytoin, and Ethotoin were given at Table 2, Tables S7–S9. All experimental spectra of Phenytoin, Mephenytoin, and Ethotoin were given comparatively at Figures 2–4.

3.2.1 | NH Stretching Vibrations

Phenytoin, mephenytoin and ethotoin are molecules that contain a hydantoin ring in their structure. In hydantoin, the NH stretching mode is usually expected at 3500–3200 cm^{-1} [42]. In the spectroscopic studies performed with molecules containing hydantoin ring, the peaks of NH stretching in the IR spectra were observed at 3461 [43] and 3475 cm^{-1} [42]. The NH stretching in the hydantoin ring of phenytoin was observed at 3476 cm^{-1}, and it was found to be consistent with the 3475 cm^{-1} value of diphenylhydantoin (phenytoin) in the literature. The NH stretching in the hydantoin ring of mephenytoin and ethotoin were respectively observed at 3460 and 3447 cm^{-1}, which is consistent with the literature value of 3461 cm^{-1}.

3.2.2 | CH Stretching Vibrations

Phenytoin, mephenytoin, and ethotoin also contain phenyl rings as well as hydantoin rings. The CH stretching of phenyl rings are observed in the region at 3100–3000 cm^{-1} [42]. In the literature, CH stretching of phenyl ring in the phenytoin were observed at 3072 and 3068 cm^{-1} (FT-IR) and 3071 (Raman) [42]. CH stretching belongs to phenytoin were observed at 3068;3038 cm^{-1} (FT-IR) and 3067;3033 cm^{-1} (Raman), experimentally. There were two types of CH stretching for mephenytoin. The first is the CH stretching of the phenyl ring, and the other is the aliphatic CH stretching. While CH stretching belong to phenyl ring of mephenytoin were observed at 3061 cm^{-1} (FT-IR) and 3075;3062;3038 cm^{-1} (Raman), aliphatic CH stretching of mephenytoin were observed at 3024;2968 (FT-IR) and 3023;2968;2947;2904 cm^{-1} (Raman). In the Raman spectrum of ethotoin, the CH stretching of phenyl ring were observed at 3059 and 3043 cm^{-1}, theoretically calculated at 3059 and 3045 cm^{-1}, respectively. The aliphatic CH stretching of ethotoin were observed at 2977;2944;2918 cm^{-1} in the FTIR spectrum and 3007;2976;2941;2904 cm^{-1} in the Raman spectrum. In addition, it was determined that the theoretical wavenumbers were also compatible with the experimental wavenumbers.

3.2.3 | C=O Stretching Vibrations

All hydantoin-based molecules have C=O stretching mode as well as N—H stretching. The aromatic C=O stretching are observed in the range of 1775–1650 cm^{-1} [42]. In the literature, CO stretching of molecules containing hydantoin ring were observed in the FT-IR spectra in the ranges of 1775–1772 and 1744–1722 cm^{-1} [17, 41–47]. In the Raman spectra, the peaks of C=O stretching were determined at similar ranges. In this study, Raman spectra were obtained for hydantoin-based molecules by using green and red lasers as well as FT-IR spectra. While the C=O stretching bands of phenytoin were observed in the FT-IR spectrum at 1774 and 1739 cm^{-1}, were observed in the Raman spectra at 1764;1735 cm^{-1} and 1771;1754 cm^{-1}. For mephenytoin, these peaks were observed at 1768 cm^{-1} in the FT-IR spectrum and at 1761;1765 and 1765 cm^{-1} in the Raman spectra. C=O stretching modes for ethotoin were defined at 1773 cm^{-1} (FT-IR) and 1765;1766;1745 cm^{-1} (Raman).

3.2.4 | CC Stretching Vibrations

The aromatic CC stretching are observed in the range of 1625–1430 cm^{-1} [44]. The aromatic CC stretching of the molecules was generally observed in the phenyl rings attached to the hydantoin ring. In the literature, the aromatic CC stretching vibrations belong to phenytoin were observed at 1598, 1493, 1450, 1448 cm^{-1} (IR) and 1602, 1586, 1497 cm^{-1} (Raman) for phenyl rings [42]. In this study, the aromatic CC stretching vibrations of the phenytoin were observed at 1597 cm^{-1} (FT-IR) and 1610, 1599, 1597, 1585, 1583 cm^{-1} (Raman). In the literature, the CC stretching vibration of phenyl ring was observed at 1287 and 1286 cm^{-1} [41, 44]. The other CC stretching vibration of phenyl ring in the phenytoin was observed in Raman spectrum at 1280 cm^{-1} in accordance with the literature. Additionally, the other CC stretching peaks of phenytoin were observed at 1031 cm^{-1} (FTIR), 1031;1032 cm^{-1} (Raman) in this study.

Another CC stretching vibrations were observed with the contribution of CCC and CCH bending modes. For mephenytoin, the aromatic CC stretching was observed 1598 cm^{-1} (FT-IR) and 1611, 1598, 1597 cm^{-1} (Raman). The other CC stretching vibrations were observed in FTIR spectrum at 1062;1031 cm^{-1} and 1063;1032 cm^{-1} in Raman spectra. The theoretical wavenumber of this stretching vibration was calculated as 1064 cm^{-1} and determined that the theoretical and experimental wavenumbers are compatible with each other. Additionally, the other CC

TABLE 2 | Hydantoin ring vibration comparison of Phenytoin, Mephenytoin, and Ethotoin.

	Reference		Phenytoin				Mephenytoin				Ethotoin				
	FTIR	FTRaman	FT-IR	Raman		Freq (Gw)	FT-IR	Raman		Freq (Gw)	FT-IR	Raman		Freq (Gw)	
				Red	Green			Red	Green			Red	Green		
Assignments	ν_{exp}	ν_{exp}	ν_{exp}	ν_{exp}	ν_{exp}	$\nu_{sca.}$ [17]	ν_{exp}	ν_{exp}	ν_{exp}	$\nu_{sca.}$ [17]	ν_{exp}	ν_{exp}	ν_{exp}	$\nu_{sca.}$ [17]	**PED assignments GAR2PED [18]**
$\nu_{NH(hydantoin)}$	3461 [43], 3475 [42]		3476	—	—	3482, 3481	3460	—	3493	3496	3447	—	—	3505	$\nu_{NH(hydantoin)}$
$\nu_{C=O(hydantoin)}$	1775 [43], 1774 [45], 1772 [42], 1736 [47]	1771 [43], 1770 [46], 1790 [42], 1760 [44], 1723 [47], 1757 [42]	1774, 1739	1764, 1735	1771, 1754	1767, 1734	1768	1761, 1745	1765	1758, 1746	1773	1765, 1745	1766	1762, 1752	$\nu_{C=O(hydantoin)} + \delta_{CNC(hydantoin)} + \nu_{CN(hydantoin)asym}$
$\nu_{CN(hydantoin)}$	1405 [41]	1425 [46]									1424	1422	1425	1410	
$\delta_{CNH(hydantoin)rock}$	1381 [47], 1377 [45]	1388 [47]	1363	1388	1383	1375	1383	1379	1383	1380	1382	1385	1384	1385	$\delta_{CNH(hydantoin)rock}$
$\delta_{CNH(hydantoin)}$		1358 [46], 1362 [42]	—	1357	1360	1354	—	—	—	—	—	—	1354	1358	$\delta_{CNH(hydantoin)} + \nu_{CN(hydantoin)}$
$\delta_{CNH(hydantoin)rock}$			—	—	1335	1333					1346	1341	1344	1349	$\delta_{CNH(hydantoin)}$
$\nu_{CN(hydantoin)} + \delta_{NCH(CH3\text{-}hydantoin)rock}$							1284	1274	1284	1272	1285	1280	1287	1287	$\nu_{CC(benzene)asym} + \delta_{NCH(hydantoin)} + \nu_{CC(benzene)} + \delta_{CCH(benzene)rock}$
$\nu_{CN(hydantoin)}$	1223 [47], 1197 [45], 1194 [42]	1200 [46], 1197 [42], 1223 [47]	—	1204	—	1209	—	1223	1235	1226	1215	—	—	1214	$\nu_{CN(hydantoin)}$
$\nu_{CC(hydantoin\text{-}benzene)}$	1197 [45]	1200 [46]										1202	1020	1194	$\nu_{CC(hydantoin\text{-}benzene)} + \nu_{CC(benzene)asym} + \delta_{CCH(benzene)rock} + \delta_{CCC(benzene)}$
$\nu_{CN(hydantoin)}$			—	—	—	—	—	—	1157	1150	—	1178	1178	1172	$\nu_{CN(hydantoin)}$
$\nu_{CN(hydantoin)}$			1099	1102	1101	1099	—	—	—	—	1106	1093	1093	1101	$\nu_{CN(hydantoin)}$
$\nu_{CN(hydantoin)}$	1045 [47] 1075 [45]	1051 [47]	1071	1062	1072	1064	—	—	—	1045	1065	—	1054	1057	$\nu_{CN(hydantoin)}$
$\nu_{CN(hydantoin)} + \delta_{CCH(CH3CH2)rock}$							1012	1003	1003	1004					
$\nu_{CN+CC(hydantoin)}$	990 [45]		982	983	984	985									
		969 [47]	—	—	—	965	—	963	—	958	—	—	—	989	$\nu_{CN(hydantoin)} + \nu_{CC(hydantoin)}$
$\Gamma_{OCNC(hydantoin)}$			935	937	939	932	936	936	936	939	—	—	—	—	$\Gamma_{OCNC(hydantoin)}$

(Continues)

TABLE 2 | (Continued)

	Reference		Phenytoin				Mephenytoin				Ethotoin				
	FTIR	FTRaman	FT-IR	Raman		Freq (Gw)	FT-IR	Raman		Freq (Gw)	FT-IR	Raman		Freq (Gw)	
				Red	Green			Red	Green			Red	Green		PED assignments GAR2PED [18]
Assignments	ν_{exp}	ν_{exp}	ν_{exp}	ν_{exp}	ν_{exp}	$\nu_{sca.}$ [17]	ν_{exp}	ν_{exp}	ν_{exp}	$\nu_{sca.}$ [17]	ν_{exp}	ν_{exp}	ν_{exp}	$\nu_{sca.}$ [17]	
$\nu_{CN(hydantoin)} + \delta_{NCN(hydantoin)}$							863	864	864	863					
$\Gamma_{CCNO} + \Gamma_{CCCN(hydantoin)}$											852	851	852	847	$\Gamma_{CCNO(hydantoin)} + \Gamma_{CCCN(hydantoin\text{-}benzene)} + \Gamma_{CNCC(hydantoin)} + \nu_{CC(hydantoin\text{-}benzene)} + \nu_{CC(benzene)} + \Gamma_{CCCH(benzene)}$
$\Gamma_{CNNO(hydantoin)}$			746	747	747	749	732	761	—	750	—	751	—	752 641	$\Gamma_{CNNO(hydantoin)} + \Gamma_{CCNC(hydantoin)}$
$\Gamma_{CNCO(hydantoin)}$							723	726	725	723					
$\delta_{NCO(hydantoin)rock}$	701 [44], 670 [45]	693 [44], 640 [46]	640	642	643	642	—	677	—	668	641	638	641	635	$\delta_{NCO(hydantoin)rock}$
$\delta_{CNC(hydantoin)}$		597 [46]	—	614	619	619	601	604	603	598	600	584	—	588	$\delta_{CNC(hydantoin)} + \nu_{CN(hydantoin)}$
$\delta_{CCN(CH3CH2\text{-}hydantoin)}$											434	442	445	437	$\delta_{CCN(CH3CH2\text{-}hydantoin)} + \delta_{NCO(hydantoin)rock} + \Gamma_{CCCC(benzene)} + \delta_{CCH(CH3CH2)rock} + \Gamma_{CCCN(CH3CH2\text{-}hydantoin)}$
$\Gamma_{CNHC(hydantoin)}$			406	421	—	411, 407	—	407	—	410	—	—	—	—	$\Gamma_{CNHC(hydantoin)}$
$\Gamma_{CNHC(hydantoin)}$			—	—	—	—	—	384	—	380	—	368	—	374	$\Gamma_{CNHC(hydantoin)}$
$\Gamma_{NCCN(hydantoin)}$			—	—	—	319	—	321	—	314	—	—	—	—	$\Gamma_{NCCN(hydantoin)}$
$\Gamma_{CCNC(hydantoin)}$			—	148	—	143	—	147	—	143	—	—	—	134	$\Gamma_{CCNC(hydantoin)} + \Gamma_{CNHC(hydantoin)}$
$\Gamma_{CCNH(hydantoin)}$			—	—	—	—	—	99	—	93	—	109	—	107	$\Gamma_{CCNH(hydantoin)} + \Gamma_{CCNC(hydantoin)}$
$\Gamma_{NCCN(hydantoin)}$		88 [46]	—	95	—	100	—	—	—	88	—	—	—	—	$\Gamma_{NCCN(hydantoin)}$

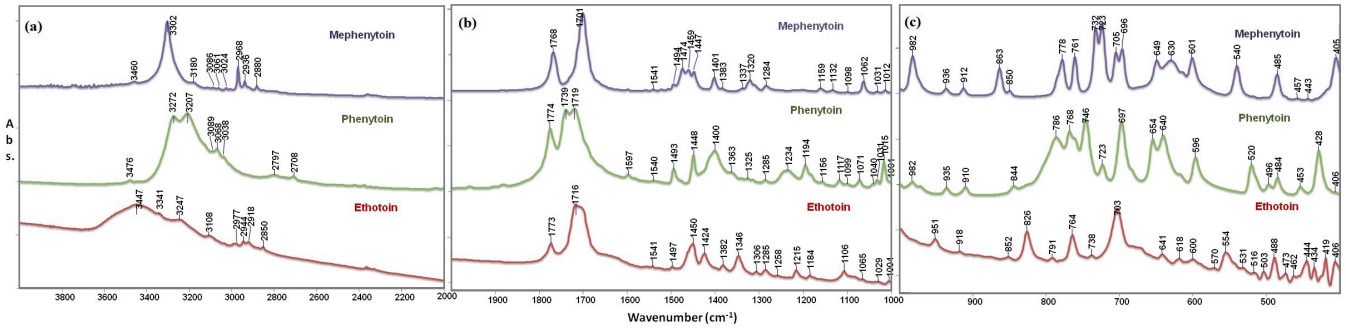

FIGURE 2 | Measured FT-IR values in (a) 4000–2000 cm^{-1}, (b) 2000–1000 cm^{-1}, and (c) 1000–400 cm^{-1} regions of Mephenyton, Phenytoin, and Ethotoin.

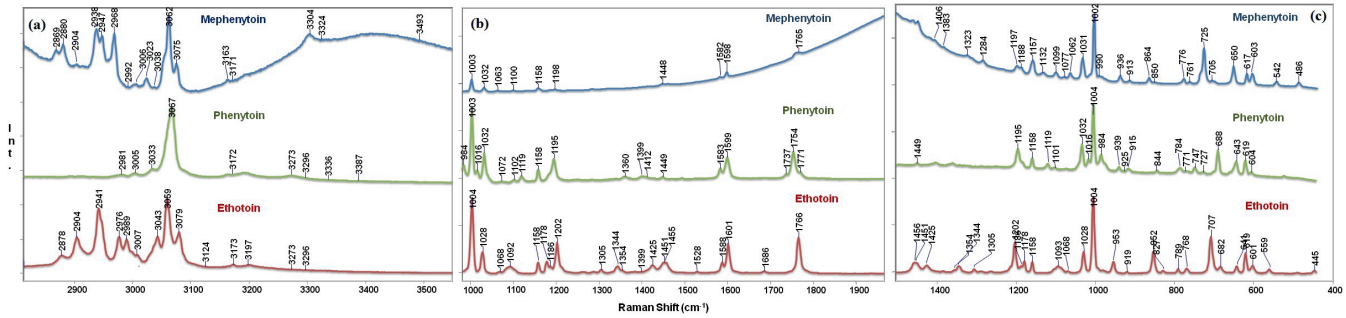

FIGURE 3 | Green laser Raman spectra of Mephenytoin, Phenytoin, and Ethotoin with the center of 3200 cm^{-1}(a), 1500 cm^{-1}(b), and 1000 cm^{-1}.

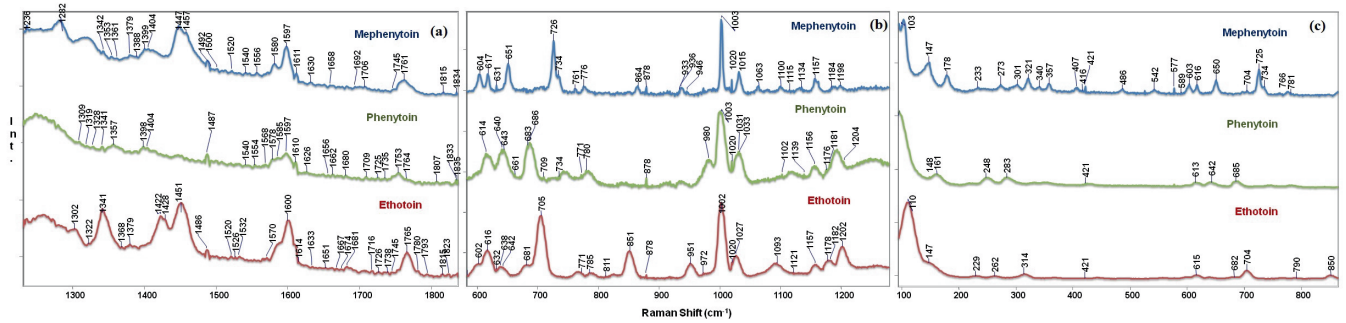

FIGURE 4 | Red laser Raman spectra of Mephenytoin, Phenytoin, and Ethotoin with the center of 1550 cm^{-1}(a), 950 cm^{-1} (b), and 500 cm^{-1}(c).

stretching peaks of mephenytoin were observed at 936 cm^{-1} in FTIR and Raman spectra.

Additionally, the aromatic CC stretching of the ethotoin were observed at 1614, 1601, 1600 cm^{-1} (Raman). The other CC stretching (CH3—CH2) vibration was observed in Raman spectrum at 1068 cm^{-1}. For ethotoin, CC stretching was observed at 1029 cm^{-1} in FTIR spectrum and 1202;1027;1028 cm^{-1} in Raman spectra, consistent with the literature. The other CC stretching was observed at 951 cm^{-1} (FTIR) and 951;953 cm^{-1} (Raman).

3.2.5 | CN Stretching Vibrations

The CC and CN stretching vibrations belong to heteroaromatic ring are observed between 1625 and 1100 cm^{-1} [42]. It is very difficult to observe the pure CN stretching vibrations in the spectra. However, within the reference range, the peaks of CN stretching were detected, with CC stretching or bending motions. The CN stretching for all hydantoin-based molecules were observed in the range of 1357–965 cm^{-1}. The CN stretching vibrations of the phenytoin were observed in the region of 1360–983 cm^{-1} and calculated in the region of 1354–965 cm^{-1}. In the literature, the peaks of CN stretching motion of hydantoin ring were observed at 1075;1045;990 cm^{-1} (IR) and 1051 cm^{-1} (Raman) [45, 47]. The peaks of CN stretching in the phenytoin spectra were observed 1071;982 cm^{-1} (FT-IR) and 1062;1072;983;984 cm^{-1} (Raman) in this study.

The CN stretching vibrations of the mephenytoin were observed in the region of 1235–863 cm^{-1} and calculated the theoretical wavenumbers in agreement with the experimental values. The peak of the movement involving NCH bending and CN stretching for hydantoin was observed at 1287 cm^{-1} in the literature [45]. The peak of CN + NCH motion of mephenytoin was observed at 1284 cm^{-1} (FTIR) and 1274;1284 cm^{-1} (Raman).

Additionally, the peak of CN + HCH motion of mephenytoin was observed at 1157 cm^{-1} in Raman spectrum. The peak of CN + CCH motion for mephenytoin was observed at 1012 cm^{-1} (FTIR) and 1003 cm^{-1} (Raman). The peaks of CN + NCN motion of hydantoin were observed at 863 cm^{-1} (FTIR) and 864 cm^{-1} (Raman) for mephenytoin.

The CN stretching vibrations of the ethotoin were observed in the region of 1425–1054 cm^{-1} and assigned considering the literature and theoretical values. The peak of CN stretching of hydantoin ring observed at 1405 cm^{-1} (IR) [41] and 1425 cm^{-1} (Raman) [46] in the literature was observed at 1424 cm^{-1} (FTIR), 1422;1425 cm^{-1} (Raman) for ethotoin in this study. Additionally, the peak of CN stretching of ethotoin was observed at 1178 cm^{-1} in Raman spectrum.

3.2.6 | Bending and Torsion Motions

The peaks of CCH bending motion for benzene ring for phenytoin are observed at 1449 cm^{-1} (IR) and 1454 cm^{-1} (Raman) in the literature [44]. In this study, the CCH bending peaks of phenytoin were observed at 1448;1340;1194;1156 cm^{-1} (IR) and 1493;1494;1451;1449;1342;1341;1195;1193;1158;1156 cm^{-1} (Raman).

The peaks of HCH bending motion for mephenytoin were observed at 1459 cm^{-1} (FTIR) and 1457;1461 cm^{-1} (Raman). The peaks of this motion for ethotoin were observed at 1450 cm^{-1} (FTIR) and 1451;1455 cm^{-1} (Raman).

The peaks of CCH bending motion of ethotoin were observed at 1184 cm^{-1} (FTIR) and 1456;1182;1186;1159;1158 cm^{-1} (Raman). The peak belonging to CCH bending and CN stretching of ethotoin was observed at 1106 cm^{-1} (FTIR) and 1093 cm^{-1} (Raman).

The peaks of CNH bending motion for hydantoin ring are observed in the range of 1388–1333 cm^{-1} in the literature [41, 45, 47]. Shyni et al. reported that the NH in-plane bending mode were observed in Raman at 1362 and 1343 cm^{-1} [42]. In this study, the CNH vibration bands for phenytoin were observed in FTIR at 1363 cm^{-1} and in Raman in the range of 1388–1335 cm^{-1}. These vibration bands for mephenytoin were observed in FTIR at 1383 cm^{-1} and in Raman at 1379 and 1383 cm^{-1}.

The CNH + CCH bands of the ethotoin were observed at 1382 cm^{-1} (FTIR) and in the range of 1385;1384 cm^{-1} (Raman). The other peak of CCH bending motion of ethotoin were observed at 1346 cm^{-1} (FTIR) and 1341;1344 cm^{-1} (Raman). The peak of CC stretching + NCH bending motions of ethotoin was observed at 1285 cm^{-1} (FTIR) and 1280;1287 cm^{-1} (Raman).

The peaks of CCC bending motion were observed at 1001 cm^{-1} (FTIR) and 1003;1004 cm^{-1} (Raman) for phenytoin. The peaks of CCCC torsion and CC stretching motion were observed at 734;727 cm^{-1} in the Raman spectra of phenytoin. Other CCCC torsion motions of phenytoin were observed at 697;520 cm^{-1} (FTIR) and 525;522 cm^{-1} (Raman). Additionally, the peaks of CCC bending motion of phenytoin were observed 685 and 688 cm^{-1} in Raman spectra.

The peaks of CCC bending motion were observed at 1004;618 cm^{-1} (FTIR) and 1002;1004;619;616 cm^{-1} (Raman) for ethotoin. The peak of CCNO and CCCN torsion motion was observed at 852 cm^{-1} in FTIR spectrum and 851;852 cm^{-1} in Raman spectra. The peak of CCCC and CCCH torsion motion was observed at 703 cm^{-1} (FTIR) and 705;707 cm^{-1} (Raman) for ethotoin. Additionally, the peak of CCCC motion was observed at 488 cm^{-1} in FTIR spectrum and 682;487 cm^{-1} in Raman spectra.

The peaks of CCCH torsion motion were observed at 982;850 cm^{-1} (FTIR) and 989;990;850 cm^{-1} (Raman) for mephenytoin. The peaks of CNNO and CNCO torsion motions of hydantoin ring of mephenytoin were observed at 732;723 cm^{-1} (FTIR) and 761;726;725 cm^{-1} (Raman). The peaks of CCCC torsion of mephenytoin were observed at 705;696;540 cm^{-1} (FTIR) and 704;705;542 cm^{-1} (Raman). The peaks of CCC bending motion of mephenytoin were 649;630 cm^{-1} (FTIR) and 651;650;631;617 cm^{-1} (Raman).

The peaks of NCO bending motion for hydantoin ring are observed at 670;642;641 cm^{-1} (IR) and at 649;648;640 cm^{-1} (Raman) in the literature [42, 44, 46]. For phenytoin, this motion was observed at 640 cm^{-1} (FTIR) and 642–643 cm^{-1} (Raman). For mephenytoin, NCO bending motion was observed at 677 cm^{-1} in Raman spectrum. For ethotoin, the peaks of this motion were observed at 641 cm^{-1} in FTIR and at 638;641 cm^{-1} in Raman spectra.

In the literature, CNC bending motion of hydantoin was observed at 597 cm^{-1} in Raman spectrum [46]. For phenytoin, the peaks of CNC bending motion were observed at 614;619 cm^{-1} in Raman spectra. For mephenytoin, this bending motion was observed at 601 cm^{-1} (FTIR) and 604;603 cm^{-1} (Raman). For ethotoin, this bending motion was observed at 600 cm^{-1} (FTIR) and 584 cm^{-1} (Raman). Additionally, the peak of CCN bending motion of ethotoin was observed at 434 cm^{-1} (FTIR) and 442;445 cm^{-1} (Raman).

3.3 | Thermodynamic Parameters

Quantum chemical calculations can provide important information about the occurrence states of chemical reactions together with the heat effects because of the difficulty of examining the heat effect thermodynamically in many organic molecules [19].

Thermodynamic parameters such as zero point vibration energy, thermal energy, specific heat capacity, entropy, and dipole moment were calculated at Gaussian 09 package program with DFT/B3LYP/6-311++G(d,p) basis set under 298.15 K and 1 atm [48]. The global minimum energies were obtained for the optimized phenytoin, mephenytoin, and ethotoin molecules with DFT/B3LYP/6-311++G(d,p) basis set are −839.0411212 a.u., −725.9115461 a.u., −686.58975664 a.u., respectively. The thermal energy, heat capacity, and entropy were calculated for all molecules. Total thermal energies and zero-point vibrational energies of the molecules were compared, it was seen that Mephenytoin has the highest values with 162.892 and 153.41834 kcal/mol, respectively. Thermodynamic parameters, thermodynamic energies, and thermochemistry provide important information in predicting the direction of chemical reactions [49, 50]. All parameters of molecules were listed on Table 3.

TABLE 3 | The calculated thermodynamic parameters of Phenytoin, Mephenytoin, and Ethotoin.

	Phenytoin	Mephenytoin	Ethotoin
Thermal energy: *E* (kJ/mol)			
Total	160.738	162.892	144.651
Translational	0.889	0.889	0.889
Rotational	0.889	0.889	0.889
Vibrational	158.961	161.114	142.874
Heat capacity: C_v (cal mol^{-1} K^{-1})			
Total	59.645	56.663	50.419
Translational	2.981	2.981	2.981
Rotational	2.981	2.981	2.981
Vibrational	53.684	50.702	44.458
Entropy: *S* (cal mol^{-1} K^{-1})			
Total	125.609	124.255	120.505
Translational	42.474	42.043	41.845
Rotational	33.226	32.238	32.009
Vibrational	49.908	49.975	46.652
Other parameters			
Total energy (a.u)	−839.0411212	−725.9115461	−686.58975664
Zero-point vibrational energy (kcal mol^{-1})	151.29227	153.41834	136.16786
Rotational constants (GHz)	0.46529	0.87906	1.37146
	0.36865	0.38425	0.35698
	0.26456	0.36339	0.31568
Rotational temperatures (Kelvin)	0.02233	0.04219	0.06582
	0.01769	0.01844	0.01713
	0.01270	0.01744	0.01515

3.4 | Mulliken Energies

Mulliken charge distribution highly related with vibrational properties of molecules. It also gives information about charge transfer in reactions [23, 51]. Due to these properties, it also provides the examination of dipole moment, polarizability, charge distributions of atoms and, chemical bond structures within the molecules [52]. Mulliken charge distribution of Phenytoin, Mephenytoin, and Ethotoin molecules calculated using the DFT-B3LYP theory level with 6-311++G(d,p) basis set is given in Table S10 and plotted in Figure 5. Mulliken charges of the molecules were examined, in the phenytoin molecule, it was determined that the C14 atom has the most positive charge compared than other atoms and the C6 atom has the most negative charge. Similarly in the literature, it was determined that the carbon atoms in the phenyl rings connected with the hydantoin ring have the most positive and the most negative values [24]. In the ethotoin molecule, it was determined that the carbon atom (C11) in the phenyl ring has the highest positive charge as in phenytoin, while the carbon atom (C4) in the hydantoin has the highest negative charge. In the mephenytoin, it was determined that the carbon atom (C3) in the hydantoin ring has the highest positive charge, while C1 atom in the CH2CH3 group has the highest negative charge. When the hydantoin rings of all three molecules were examined, it was determined that both oxygen atoms had negative charges due to their strong electronegativity. All nitrogen atoms in the hydantoin ring of phenytoin, and mephenytoin had negative charge, while the one of nitrogens in the ethotoin had negative charge. In summary, it was seen that most of the C, N, and O atoms have negative charges while the hydrogen atoms have positive charges. Especially, H atoms in hydantoin ring had maximum positive charge than the other H atoms, as seen in all three molecules, because the presence of electronegative atom nitrogen. Some carbon atom of phenytoin had the highest negative Mulliken charge, followed by O12 and N10 atoms in this study, while the oxygen atoms had the maximum negative Mulliken charges in a study conducted with phenytoin derivative [23]. When compared with the study conducted by Sevvanthi, Muthu, and Raja, it was determined that most of the carbon atoms had a negative mulliken charge, followed by nitrogen and oxygen atoms, similar to this study [24]. Another hydantoin-derived compound has been reported to be more negative than nitrogen and oxygen when looking at mulliken charges [53].

3.5 | MEP Analysis

Molecular electrostatic potential (MEP) gives an information about charge distributions of molecule. Molecular interactions are related to charge distributions of molecule. MEP analyses for phenytoin, mephenytoin, and ethotoin were carried out and

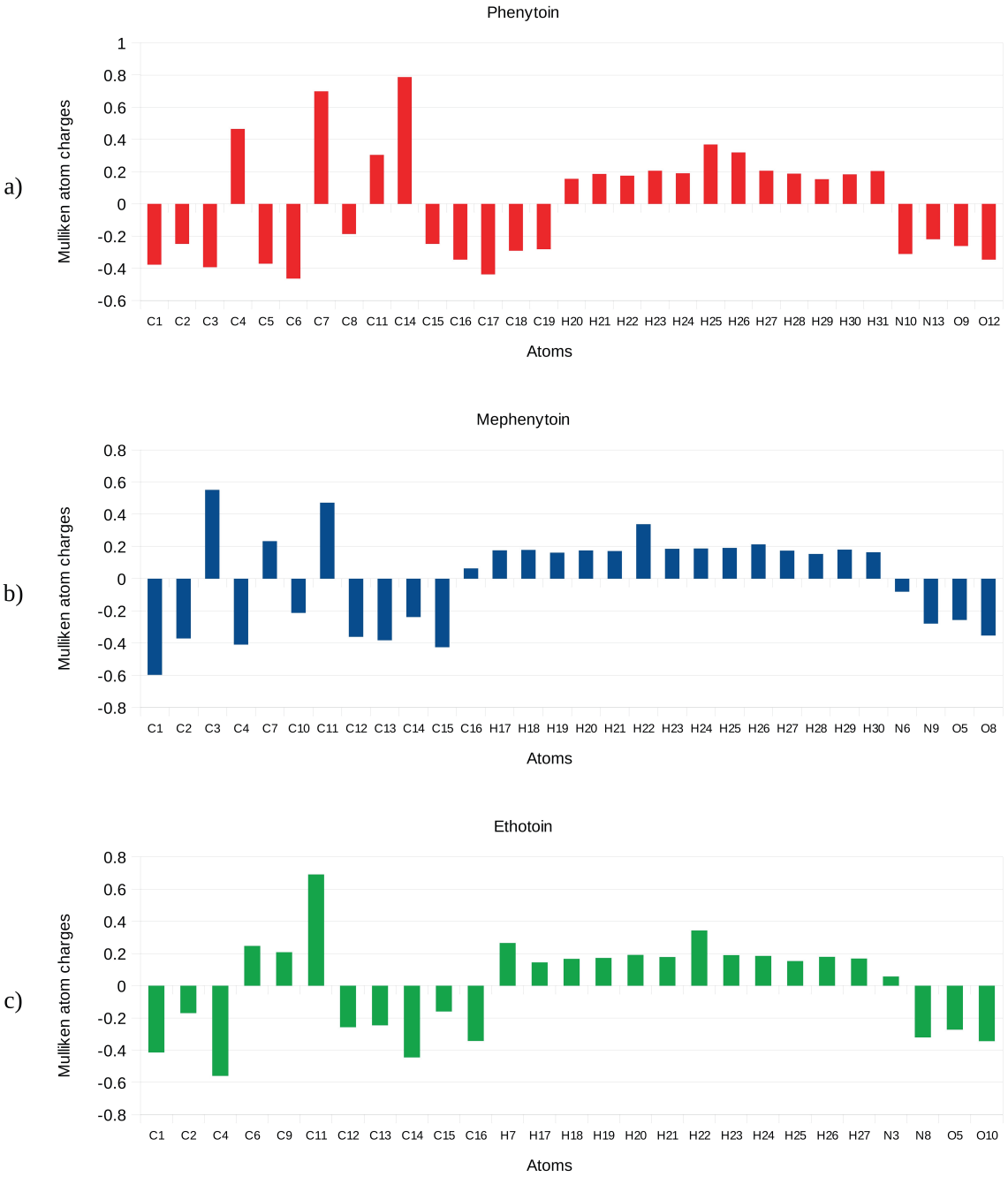

FIGURE 5 | Mulliken charge graphs of Phenytoin, Mephenytoin, and Ethotoin (energies in terms of a.u. unit).

shown in Figure 6. When the maps of the three molecules were examined, it was determined that the hydantoin rings contain the richest and the poorest regions in terms of electron, that is, the chemically active sites. As can be seen from the Figure 6, the negative electrostatic potential regions were mainly localized on CO group in the hydantoin rings, indicating possible sites for electrophilic attack. The positive electrostatic potential regions were mainly localized on NH group in the hydantoin rings, indicating possible sites for nucleophilic attack.

In the mapping for phenytoin, the potential energy values were determined as ±0.05315 a.u. The negative potentials were localized on the O9 and O12 atoms in the hydantoin ring, while the positive potential regions were localized on the H25 atoms attached to N10 and H26 atoms attached to N13. In the mapping for mephenytoin, the potential energy values were determined as ±0.05569 a.u. The negative potentials were localized on the O5 and O8 atoms in the hydantoin ring of mephenytoin, while the positive potential region was on the H22 atom attached to the N9 in the hydantoin-ring. In the mapping for ethotoin, the potential energy values were determined as ±0.058 a.u. The negative potentials were localized on the O5 and O10 atoms in the hydantoin ring of ethotoin, and the positive potential region was on the H22 atom attached to N8 in the hydantoin ring. In molecular docking analysis, the interactions of the receptor and the ligand are related to the recognition of their molecular surfaces [54]. Considering that hydantoin rings stand out in the electrostatic potential maps of all three molecules in MEP

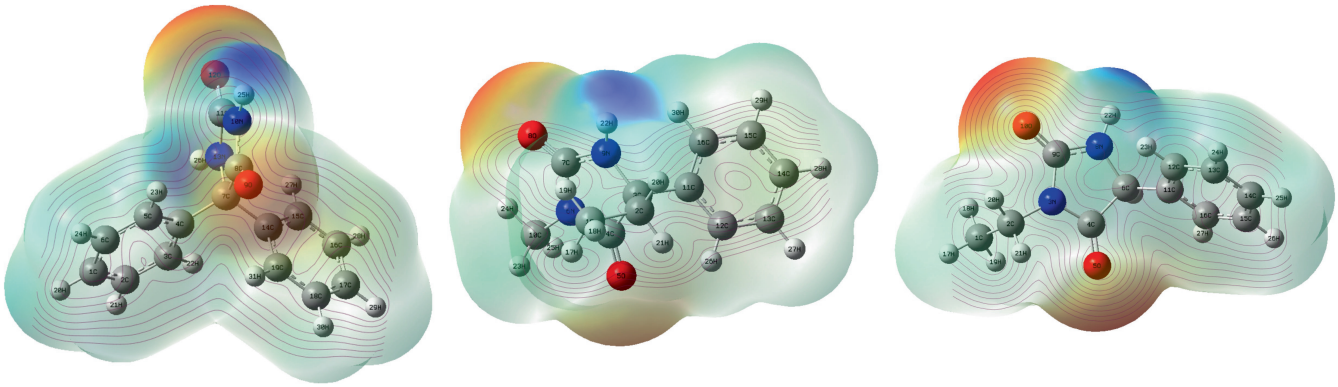

a) b) c)

FIGURE 6 | MEP maps of (a) Phenytoin, (b) Mephenytoin, and (c) Ethotoin.

analysis, the fact that all molecules make salt bridges and metal interactions from hydantoin rings in the molecular docking study with the GABA-AT receptor seems to be related to the MEP map.

3.6 | HOMO-LUMO Analysis

HOMO and LUMO are the main orbitals that participate in chemical reactions. HOMO-LUMO (ΔE) energy gap inform about the charge transfer interaction within the molecule. If ΔE gap is high, chemical reactivity is low [55, 56]. HOMO-LUMO analysis are used to obtain information about the optic and electronic properties of molecules. HOMO and LUMO are related to electron donating and accepting capacity, respectively [57]. LUMO (the lowest unoccupied molecular orbital) energy is related to the electron affinity, while HOMO (the highest occupied molecular orbital) energy is related to the ionization potential.

HOMO, LUMO figures, their energies and related values of the drug molecules given in the Figure 7 and Table 4. The HOMO-LUMO energy gap (ΔE) is related to obtaining values related to various properties such as chemical reactivity, electron affinity, electronegativity, and chemical hardness [58]. Considering the ΔE energy gap, it can be said that if ΔE gap of a molecule is low, the molecule has the low chemical hardness, molecules with lower chemical hardness are more reactive. In this study, it was clearly seen by investigating the chemical hardness and ΔE gap values that phenytoin is more reactive than other hydantoin-based molecules. When the chemical hardness values of hydantoin-based drugs were examined, it was determined that the highest value was Mephenytoin molecule, therefore it had lower reactivity. In the study conducted with hydantoin using the B3LYP/6-311++G(d,p) basis set [58], it was observed that the energy gap of hydantoin was much larger than that of hydantoin-based drugs (ethotoin, mephenytoin, and phenytoin). Therefore, hydantoin-based drugs tend to be more reactive than hydantoin molecule. Additionally, ΔE energy gaps of hydantoin-based molecules in our study was similar to ΔE energy gaps of hydantoin-based compounds in the literature [23, 59]. Additionally, in the study conducted by Serdaroglu and Ortiz, HOMO, and LUMO energies of phenytoin were calculated at 6-311++G(d,p) basis set. When it was compared all energies with our study, it was seen that obtained energy values were exactly the same [60].

3.7 | NBO Analysis

NBO analysis provides information such as intramolecular and intermolecular bonding and charge transfer [61]. NBO analyses of Phenytoin, Mephenytoin, and Ethotoin molecules were performed at Gaussian 09 package program with the DFT/B3LYP/6-311++G(d,p) basis set and all information obtained was listed in Table 5, Tables S11–S14. $E(2)$ stabilization energies were calculated for hydantoin-based molecules and it was determined that the highest values belonged to the interactions in the hydantoin ring, shown in Table 5.

The highest stabilization energies were obtained as a result of electron density transitions from the lone pairs of nitrogens in the hydantoin ring to the pi anti-bond orbitals of the C=O groups in the hydantoin ring group. The highest stabilization energy of the Phenytoin molecule with 56.32 kcal/mol, belongs to the transition from LP (1) N10 to BD*(2) C8-O9. The highest stabilization energy of the Mephenytoin molecule with 58.25 kcal/mol belongs to the transition from LP (1) N6 to BD*(2) C4-O5. The highest stabilization energy of the ethotoin molecule was found to be 57.60 kcal/mol. This energy belongs to the electron density transition from LP (1) N8 to BD*(2) C9-O10. In the study of the new phenytoin derivative with phenytoin conducted by Guerrab et al., it was reported that the best stabilization energies belong to the electron density transitions from the lone pairs of nitrogens to pi antibody orbitals of the CO in the hydantoin ring [23]. The other important electron density transitions were from the lone pairs of oxygens in the ring to the sigma antibonding orbitals of N—C and C—C in the ring.

In studies with 5-methylhydantoin and 1-methylhydantoin in the literature, it was reported that the best stabilization energies belonged to the electron density transitions from the lone pairs of nitrogens to pi antibody orbitals of the CO in the hydantoin ring. Other important electron density transitions were from the lone pairs of oxygens in the hydantoin ring to the sigma antibody

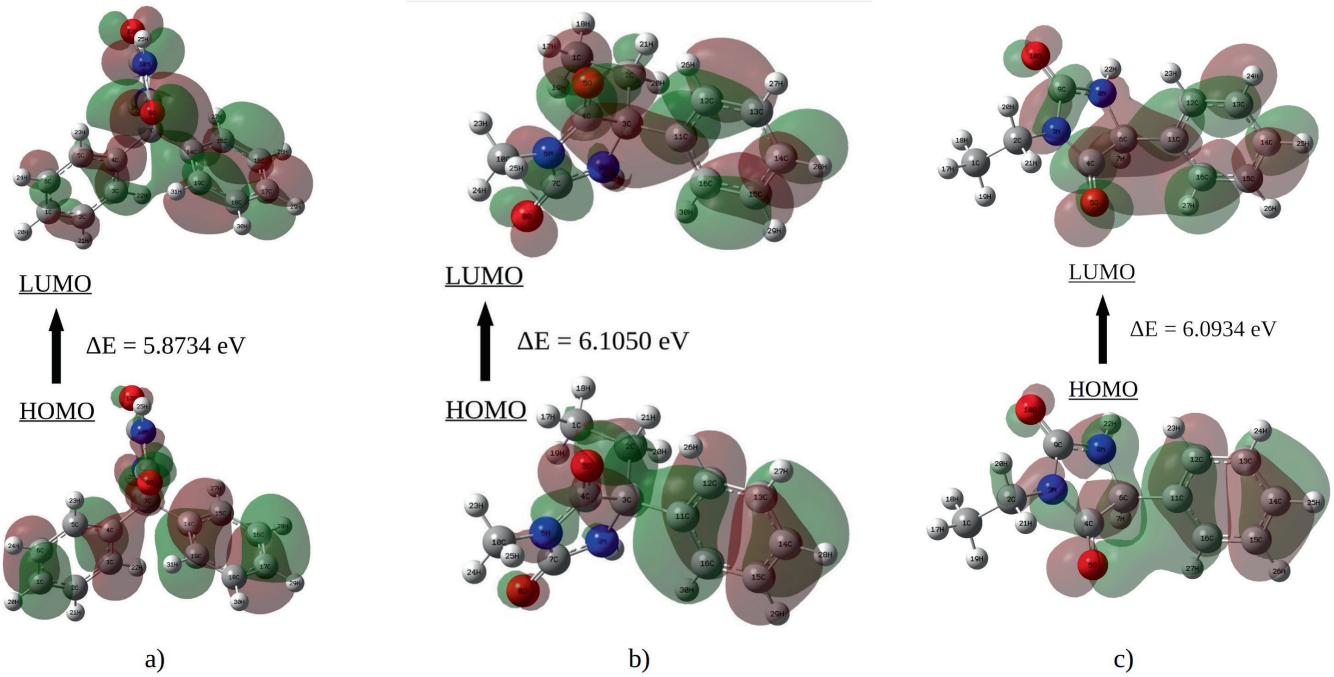

FIGURE 7 | HOMO-LUMO energy gaps of (a) Phenytoin, (b) Mephenytoin, and (c) Ethotoin.

TABLE 4 | Ionization potential, electron affinity, electronegativity, chemical hardness, chemical softness, and HOMO-LUMO gap values of Phenytoin, Mephenytoin, and Ethotoin molecules.

		Energy (eV)		
Vacuum	**DFT/B3LYP/6311++G(d,p)**	**Phenytoin**	**Mephenytoin**	**Ethotoin**
HOMO energy	E_{HOMO}	−7.0614	−7.0888	−7.1234
LUMO energy	E_{LUMO}	−1.1878	−0.9837	−1.0299
Ionization potential	$I = -E_{HOMO}$	7.0614	7.0888	7.1234
Electron affinity	$A = -E_{LUMO}$	1.1878	0.9837	1.0299
Electronegativity	$\chi = (I + A)/2$	4.1246	4.0363	4.0767
Chemical potential	$\mu = -(I + A)/2$	−4.1246	−4.0363	−4.0767
Chemical hardness	$\eta = (I - A)/2$	2.9368	3.0526	3.0467
ΔE (gap)	$E_{LUMO} - E_{HOMO}$	5.8736	6.1051	6.0934

orbitals in the hydantoin ring [62, 63]. Consequently, in our study, it was determined that the high stabilization energy $E(2)$ values are an indication of the high interactions between the electron donors and acceptors in the hydantoin ring. Considering the $E(2)$ energies of the three hydantoin-based drugs in this study (see Table 5), it has been observed that nitrogen atoms with high E(2) energy play an important role in the active site interactions obtained as a result of molecular docking analysis.

3.8 | Molecular Docking Analyses

Three hydantoin-based molecules (Phenytoin, Mephenytoin, Ethotoin) were selected for molecular docking analyses with GABA-AT receptor. The results of binding energies and close interactions between ligand and receptor were shown in Figure 8. The pdb taken from the Swiss model is regular and ordered, and there are nine differences in the order of the residues in the pdb (PDB ID: 4Y0D) taken from the protein data bank.

The (1*S*,3*S*)-3-amino-4-difluoromethylene-1-cyclopentanoic acid (CPP-115) as a ligand interacted with Cys-135 residue in the Gamma-aminobutyric acid aminotransferase [25]. In the studies of GABA-AT receptor- and hydantoin-based molecules, Phenytoin formed four salt bridge and one metal coordination interactions with the receptor binding site. The binding site interactions was given in Figure 8a. The protonated N^+H_2 part made salt bridge interactions (3.37 and 4.97 Å) with Cys-126 which indicated by C126 in the Swiss model pdb and expressed as Cys-126 that corresponds to Cys-135 residue in the protein data bank pdb file. The Fe2/S2 inorganic cluster also made one salt bridge interaction (4.48 Å) with the same part of the Phenytoin. Another salt bridge interaction and metal coordination interaction were occurred between the Fe2/S2 inorganic cluster and O atom with 2.29 Å, respectively. Mephenytoin,

TABLE 5 | Second-order perturbation theory analysis of Fock matrix based on NBO of Phenytoin, Mephenytoin, and Ethotoin molecule.

Phenytoin				
Donor NBO (*i*)	**Acceptor NBO (*j*)**	***E*(2) (kcal/mol)**	***E*(*j*)-*E*(*i*) (a.u.)**	***F*(*i*,*j*) (a.u.)**
LP (1) N10	BD*(2) C8-O9	56.32	0.29	0.117
LP (1) N13	BD*(2) C11-O12	52.14	0.29	0.113
LP (1) N10	BD*(2) C11-O12	46.26	0.29	0.104
LP (2) O12	BD*(1) N10-C11	28.36	0.64	0.122
LP (2) O9	BD*(1) C8-N10	27.19	0.70	0.125
LP (2) O12	BD*(1) C11-N13	24.71	0.69	0.120
LP (2) O9	BD*(1) C7-C8	23.14	0.58	0.105
BD (2) C18-C19	BD*(2) C14-C15	20.88	0.28	0.069
BD (2) C1-C6	BD*(2) C4-C5	20.83	0.28	0.069
BD (2) C2-C3	BD*(2) C4-C5	20.66	0.29	0.069
Mephenytoin				
Donor NBO (*i*)	**Acceptor NBO (*j*)**	***E*(2) (kcal/mol)**	***E*(*j*)-*E*(*i*) (a.u.)**	***F*(*i*,*j*) (a.u.)**
LP (1) N6	BD*(2) C4-O5	58.25	0.28	0.117
LP (1) N9	BD*(2) C7-O8	57.48	0.28	0.117
LP (1) N6	BD*(2) C7-O8	49.48	0.28	0.105
LP (2) O8	BD*(1) N6-C7	28.29	0.64	0.122
LP (2) O5	BD*(1) C4-N6	26.78	0.71	0.125
LP (2) O8	BD*(1) C7-N9	24.39	0.70	0.120
LP (2) O5	BD*(1) C3-C4	22.07	0.60	0.104
BD (2) C12-C13	BD*(2) C11-C16	21.01	0.28	0.069
BD (2) C14-C15	BD*(2) C11-C16	20.33	0.28	0.068
BD (2) C12-C13	BD*(2) C14-C15	20.28	0.28	0.068
Ethotoin				
Donor NBO (*i*)	**Acceptor NBO (*j*)**	***E*(2) (kcal/mol)**	***E*(*j*)-*E*(*i*) (a.u.)**	***F*(*i*,*j*) (a.u.)**
LP (1) N8	BD*(2) C9-O10	57.60	0.28	0.117
LP (1) N3	BD*(2) C4-O5	56.96	0.28	0.116
LP (1) N3	BD*(2) C9-O10	50.16	0.28	0.106
LP (2) O10	BD*(1) N3-C9	28.04	0.64	0.121
LP (2) O5	BD*(1) N3-C4	26.87	0.70	0.124
LP (2) O10	BD*(1) N8-C9	24.83	0.70	0.120
LP (2) O5	BD*(1) C4-C6	23.17	0.60	0.107
BD (2) C15-C16	BD*(2) C11-C12	21.31	0.28	0.069
BD (2) C13-C14	BD*(2) C11-C12	20.59	0.28	0.068
BD (2) C15-C16	BD*(2) C13-C14	20.28	0.28	0.068

also settled in the same binding site and showed salt bridge (4.79 and 2.15 Å) and metal coordination interactions (2.15 Å) with the inorganic cluster shown in Figure 8b. Ethotoin was shown best binding energy values with −6.68 kcal/mol and best interactions with GABA-AT residues. The Cys-126 (3.86 Å) residue has entered a salt bridge interaction with the N^+H_2 part of the molecule. The Fe2/S2 inorganic cluster had two salt bridge interactions with N^+H_2 part (4.06 Å) and N^+H part (4.65 Å) of the Ethotoin seen in Figure 8c. The Fe2/S2 inorganic cluster also effectuated two salt bridge interactions with O atom (2.21 Å). Additionally, Phenytoin, Mephenytoin, and Ethotoin gave binding energies of −5.95, −5.55, and −6.68 kcal/mol, respectively with GABA-AT receptor as a result of molecular docking study.

In the study [64] of in silico identification of new C-15 fluoro isosteviol derivatives for GABA-AT inhibition, it was revealed that Cys135 was noticed forming different interactions. Isosteviol

PDB ID	Phenytoin	Mephenytoin	Ethotoin
4Y0D	Binding Affinity: -5.95 kcal/mol (a)	Binding Affinity: -5.55 kcal/mol (b)	Binding Affinity: -6.68 kcal/mol (c)

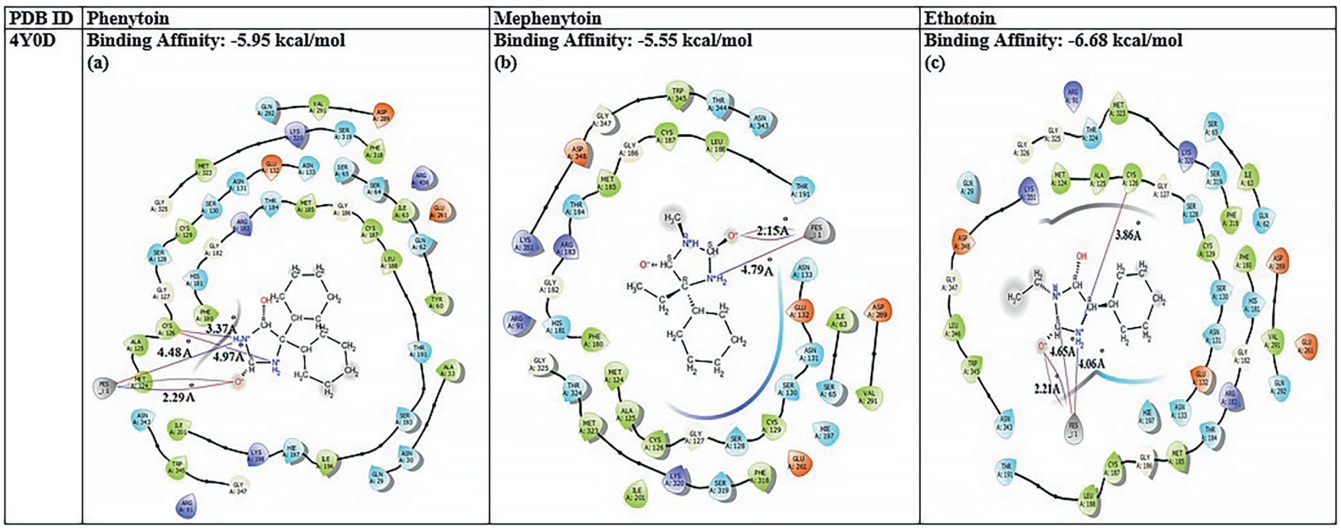

FIGURE 8 | Binding energies and close interactions of hydantoin-based molecules.

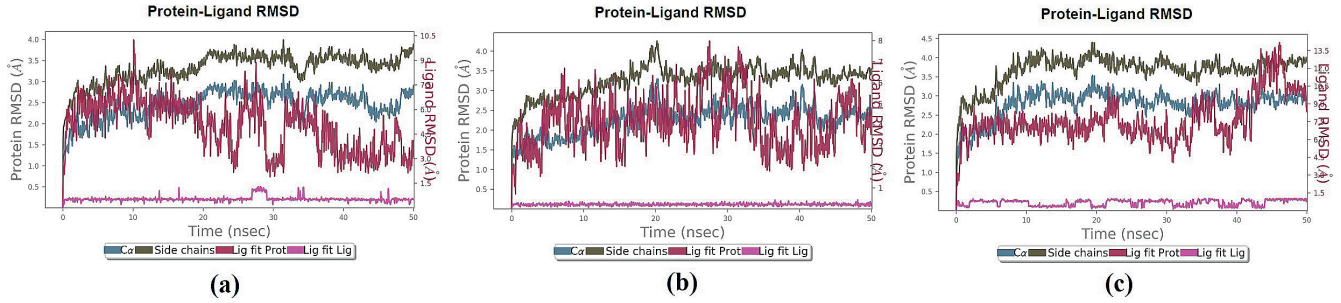

FIGURE 9 | RMSD graphs of the Ethotoin (a), Mephenytoin (b), and Phenytoin (c) complexes.

exhibited coupling with a binding energy of −7.41 kcal/mol, showing hydrogen bond interaction with Lys329 and alkyl interaction with Cys135 in the active site of 1OHW. All isosteviol analogs against 4ZSW have been reported to show tight binding capacity with binding energy lower than −5.79 kcal/mol. In the same study, it was reported that there is a hydrophobic interaction with the Cys135 residue of the 4ZSW active site.

In the literature, the molecular docking study conducted by Shallangwa et al. was carried out with GABA-AT receptor and some antiepileptic compounds [65]. It was observed that phenytoin in this study had a much better binding energy to GABA-AT compared to the binding energies of the ligands in which the docking study was performed by Shallangwa, Uzairu, and Abdulfatai. When the evaluation was made for mephenytoin and ethotoin, it was determined that the binding energy of carbamazepine used in the treatment of anti-epilepsy to GABA-AT was the same as ethotoin, and mephenytoin had a better binding energy. Another antiepileptic drug vigabatrin was docked with GABA-AT and obtained −4.4 kcal/mol binding energy [66]. It was observed that all three hydantoin-based molecules tend to bind better to GABA-AT compared with carbamazepine, vigabatrin and valproate, which are anti-epilepsy drugs.

3.9 | MD Analysis

All complexes' structures were taken from the molecular docking result for MDs studies. The MD simulations were run three times using the Desmond simulation package of the Schrödinger program to show the stability of the system by monitoring interactions of all complexes. The ethotoin-4-aminobutyrate aminotransferase complex was neutralized by adding 41 Na^+ and CI^- ions. The mephenytoin-4-aminobutyrate aminotransferase complex was neutralized by adding 60 Na^+ and 59 CI^- ions. The phenytoin-4-aminobutyrate aminotransferase complex was neutralized by adding 41 Na^+ and CI^- ions. Constant temperature and pressure were maintained at 300 K temperature and 1 bar pressure. After all preparations are completed, MD simulations of the system were performed for 50 ns.

The structural stability of 4-aminobutyrate aminotransferase and the receptor-ligand complexes were examined during simulation by analyzing root mean square deviation (RMSD) (see Figure 9). The RMSD graphs were monitorized during the simulation. RMSD values of Cα atom were investigated for all complexes concerning its initial structure to trace the effect of the hydantoin-based drug molecules (ethotoin, mephenytoin, and phenytoin) on the structural stability of 4-aminobutyrate aminotransferase during the simulations.

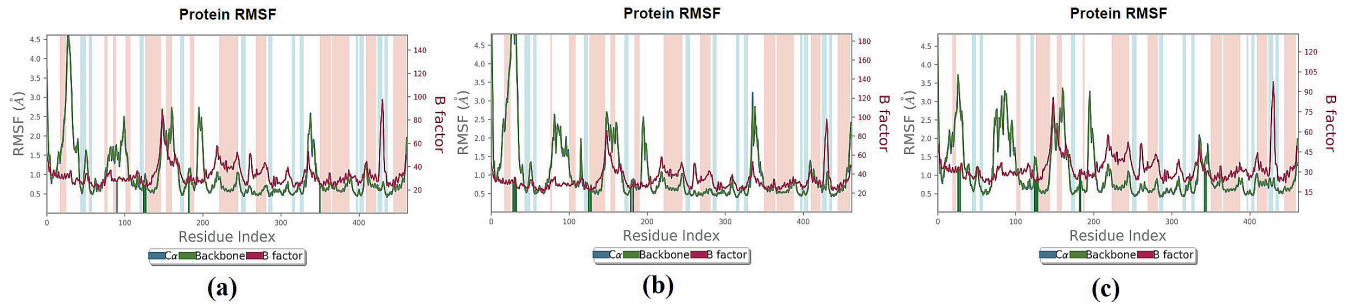

FIGURE 10 | RMSF graphs of the Ethotoin (a), Mephenytoin (b), and Phenytoin (c) complexes.

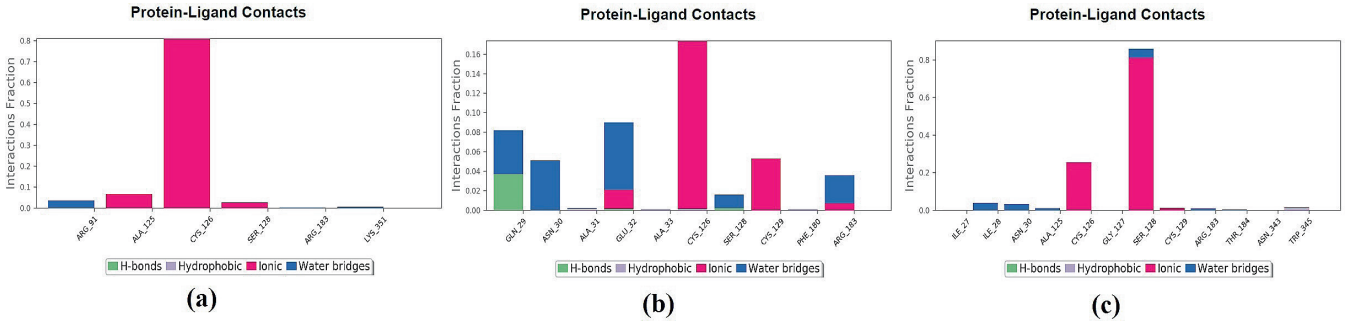

FIGURE 11 | Close interactions of the Ethotoin (a), Mephenytoin (b), and Phenytoin (c) complexes.

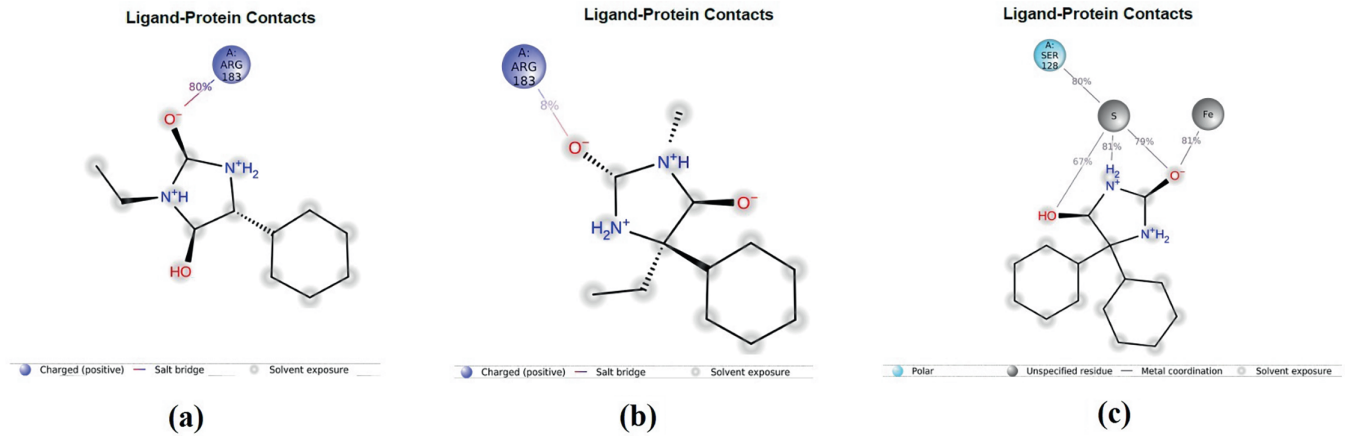

FIGURE 12 | Contacts of the Ethotoin (a), Mephenytoin (b), and Phenytoin (c) complexes.

From RMSD graph, the information of the hydantoin-based drug molecules stabilities in the binding pocket and internal fluctuations of the molecules atoms was obtained. When RMSD graphs were investigated, it was followed that the RMSD of 4-aminobutyrate aminotransferase fluctuated in a certain region of RMSD value for 50 ns and was found to tend to remain stable. The RMSD of the hydantoin-based drug molecule in the 4-aminobutyrate aminotransferase-hydantoin-based drug molecule complex was given with "Lig fit Prot" in the RMSD graph.

Root mean square fluctuation (RMSF) give the information about the local changes along the receptor chain. The most fluctuating receptor residues during the simulation are indicated by the RMFS peaks. Residues of 4-aminobutyrate aminotransferase interacting with the hydantoin-based drug molecule were indicated by vertical lines in green (see Figure 10).

The hydantoin-based drug molecules and 4-aminobutyrate aminotransferase interactions were given with bar charts and provided the information about interaction categorization like Hydrogen Bonds, Hydrophobic, Ionic, and Water Bridges. First, we examined ethotoin complex and determined ethotoin made ionic interactions and water bridges with 4-aminobutyrate aminotransferase (see Figure 11a). Ethotoin made ionic interaction with Cys-216, Ser-128, and Ala-25 residues of 4-aminobutyrate aminotransferase and water bridges with Arg-91, Arg-183, and Lys-351 residues. When we looked at bar chart of ethotoin complex, we observed that ionic interactions were dominant, especially. We can say that ethotoin

TABLE 6 | Drug-likeness values obtained from SwissADME servers of Phenytoin, Mephenytoin, and Ethotoin.

Swissadme properties			
Physicochemical properties	**Phenytoin**	**Mephenytoin**	**Ethotoin**
Polar surface area	58.2 Å^2	49.41 Å^2	49.41 Å^2
No. of H-bond acceptors	2	2	2
No. of H-bond donors	2	1	1
Molar refractivity	77.5	67.53	62.84
Rotatable bond count	2	2	2
Heavy atom count	19	16	15
Aromatic heavy atom count	12	6	6
Lipinski's rule of five	Yes	Yes	Yes
Bioavailability	Yes	Yes	Yes
MW	252.27 g/mol	218.25 g/mol	204.23 g/mol
Lipophilicity			
LogPO/W(iLOGP)	1.68	2.05	1.82
LogPO/W(XLOGP3)	2.47	1.69	1.05
LogPO/W(WLOGP)	0.9	0.6	0.21
LogPO/W(MLOGP)	1.61	1.46	0.77
LogPO/W(SILICOS-IT)	2.42	1.59	1.13
Consensus LogPO/W	1.81	1.48	1
Water solubility			
Log S (ESOL)	−3.3	−2.4	−1.93
Log S (Ali)	−3.34	−2.34	−1.68
Log S (SILICOS-IT)	−5.62	−3.57	−2.96
Pharmacokinetics			
GI absoption	High	High	High
BBBpermeant	Yes	Yes	No
CYP2C9 inhibitor	No	No	No
Log KP	−6.09 cm/s	−6.43 cm/s	−6.8 cm/s
Druglikeness			
Lipinski	Yes, 0 violation	Yes, 0 violation	Yes, 0 violation
Ghose	Yes	Yes	Yes
Veber	Yes	Yes	Yes
Muegge	Yes	Yes	Yes
Bioavailability score	0.55	0.55	0.55

and Cys-126 residue interacted during 80% of the simulation time. Mephenytoin made ionic, hydrophobic, hydrogen bond interactions, and water bridges with 4-aminobutyrate aminotransferase (see Figure 11b). In the mephenytoin complex, we observed that ionic interaction and water bridges were dominant. Like ethotoin, ionic interaction with Cys-126 residue was prominent in the mephenytoin complex simulation. In addition, it was determined that ethotoin and mephenytoin formed a salt bridge with Arg-183 residue of 4-aminobutyrate aminotransferase (see Figure 12). At the MD simulation of phenytoin complex, Cys-126 and Ser-128 residues were observed to interact for a long time with phenytoin during the simulation, in which ionic interactions were particularly prominent (see Figure 11c). The other ionic interaction was found to be with the Cys-129 residue, such as mephenytoin.

TABLE 7 | ADME, drug-likeliness, and toxicity values obtained from the PreADMET server of Phenytoin, Mephenytoin, and Ethotoin.

ADME	Phenytoin	Mephenytoin	Ethotoin
BBB	0.93	0.59	0.56
Buffer_solubility_mg_L	1046.76	3611.22	6588.48
Caco2	21.12	21.22	21.2
CYP_2C19_inhibition	Non	Non	Non
CYP_2C9_inhibition	Non	Non	Non
CYP_2D6_inhibition	Non	Non	Non
CYP_2D6_substrate	Non	Non	Non
CYP_3A4_inhibition	Non	Non	Non
CYP_3A4_substrate	Weakly	Non	Non
HIA	92.53	94.74	94.56
MDCK	140.43	43.61	22.08
Pgp_inhibition	Non	Non	Non
Plasma_Protein_Binding	96.58	81.55	46.29
Pure_water_solubility_mg_L	46.52	633.54	1781.05
Skin_Permeability	−3.67	−3.22	−3.63
SKlogD_value	2.15	1.64	1.13
SKlogP_value	2.15	1.64	1.13
SKlogS_buffer	−2.38	−1.78	−1.49
SKlogS_pure	−3.73	−2.54	−2.06
Druglikeness			
Rule_of_Five	Suitable	Suitable	Suitable
Rule_of_Five_Violation_Fields			
Rule_of_Five_Violations	0	0	0
Toxicity			
Ames_test	Mutagen	Mutagen	Mutagen
Carcino_Mouse	Positive	Negative	Negative
Carcino_Rat	Negative	Negative	Negative
hERG_inhibition	Low_risk	Medium_risk	Medium_risk

3.10 | ADME Profile

ADME (absorption, distribution, metabolism, and excretion) analysis is very important for drug candidate molecules and provides pharmacokinetic information about the molecules. ADME profiles of hydantoin-based drugs were determined by using SwissADME and PreADMET servers and were given in Tables 6 and 7.

Among oral drug candidates, most of the candidates which passed the Phase II clinical stage were examined and four physicochemical parameters were determined by Lipinski. These parameters called Lipinski's rule of 5 provide information about oral drug potential. According to Lipinski's rule of 5 [67], for a molecule to be considered as a drug, its molecular weight should be less than 500 g/mol, have no more than 5 hydrogen bond donors, have no more than 10 hydrogen bond acceptors, and its octanol/water partition coefficient should not be greater than 5. Phenytoin, Mephenytoin, and Ethotoin were found to be molecules that comply with the Lipinski rule within the framework of the features determined by SwissADME and PreADMET servers. When it was examined the four parameters in detail for all molecules, the molecular weights of Phenytoin, Mephenytoin, and Ethotoin were determined as 252.27, 218.25, and 204.23 g/mol, respectively. Hydrogen bond donors and acceptors numbers of all molecules were obtained within the limits of Lipinski rules. Octanol/water partition coefficients were determined as 1.81, 1.48, and 1 for Phenytoin, Mephenytoin, and Ethotoin, respectively. For oral intake, gastro-intestinal absorption was stated to be high for all molecules in the SwissADME server, while the oral absorption percentages were calculated as 92.53%, 94.74%, and 94.56% for Phenytoin, Mephenytoin, and Ethotoin in the PreADMET server. The Caco-2 cell model, which is one of the reliable in vitro models for the prediction of oral drug absorption, was used in the PreADMET server, and the values calculated for Phenytoin, Mephenytoin, and Ethotoin molecules were determined to be in the mid-permeability range [68]. The blood–brain barrier separates the brain from the systemic blood circulation and protects the CNS. Drugs developed for the CNS must pass the BBB [69]. For other drugs not to affect the CNS, BBB penetrations must be very low. In the PreADMET server, blood brain barrier (BBB) penetration values of phenytoin, mephenytoin, and

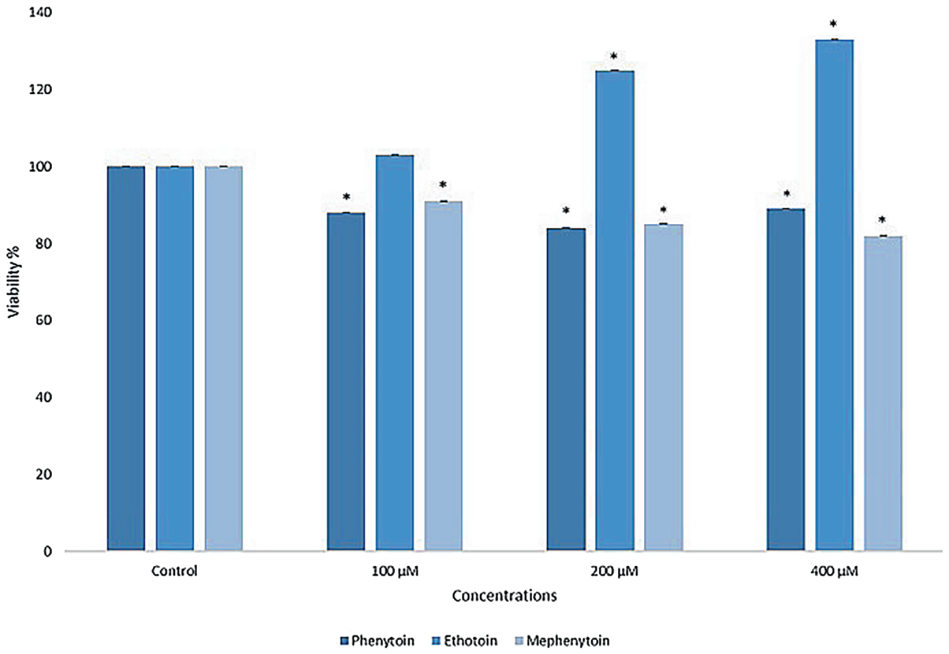

FIGURE 13 | Cell viability results of phenytoin, ethotoin, and mephenytoin on U-87 cell lines for 24 h (*$p < 0.05$).

ethotoin were obtained as 0.93, 0.59, and 0.56 and determined that they may be CNS active compounds [70]. Polar surface area (PSA) is a very important parameter in physical chemistry studies for drug discovery because PSA is used to characterize the transport process of drug molecules, like the octanol–water partition coefficient, and PSA can be related to various causes of drug absorption [71]. The PSAs for Phenytoin, Mephenytoin, and Ethotoin were determined as 58.2, 49.41, and 49.41 $Å^2$, respectively. The skin permeability values of the molecules were determined as −6.09, −6.43, and −6.8 cm/s for phenytoin, mephenytoin, and ethotoin, respectively. The more negative the skin permeability value is, the lower the skin permeability means [31]. Some drugs can be inhibited or induced Cytochrome P450 enzymes. These conditions may cause drug–drug interactions and cause undesirable reactions [72]. Phenytoin, mephenytoin, and ethotoin molecules did not inhibited CYP450 enzymes in the results of PreADMET and SwissADME servers. As a result of ADME analyses, hydantoin-based molecules are suitable for oral intake, CNS active and have no drug–drug interaction problem.

3.11 | In Vitro Studies

MTT assay was performed to evaluate the cytotoxic activity of Phenytoin, ethotoin, mephenytoin on U-87 glioblastoma cell line at 100, 200, and 400 µM concentrations for 24 h experimental duration (for phenytoin %88, %84, and %89, respectively; for Ethotoin %103, %125, and %133, respectively; Mephenytoin %91, %85, and %82, respectively) (see Figure 13). It was observed that mephenytoin showed concentration-dependent cytotoxic effect on U-87 cell line compared to control (*$p < 0.05$) while concentration dependent proliferation observed in ethotoin-treated group. It was determined that cell viability was decreased in the Phenytoin applied group compared to the control group. According to the 24-h experiment results, it was determined that the phenytoin and mephenytoin applied group showed a toxic effect against U-87 cells, while the ethotoin applied group showed proliferation. In a study conducted by Lee et al. [14] with antiepileptic drugs, it was reported that U-87 MG and T98G cells administered phenytoin showed growth inhibition after 70 h. In the study conducted by de Jonge et al. [73], when phenytoin was applied to different glioma cell lines, IC50 values were determined to be in the range of 0.19–0.48 mM at the end of 5 days. Considering these literatures, the results we obtained in our study are similar to other studies.

4 | Conclusion

In this study, the structural and pharmacokinetic properties of hydantoin-based drug molecules such as phenytoin, mephenytoin, and ethotoin were evaluated. The studies started by optimizing phenytoin, mephenytoin, and ethotoin. Theoretical vibration wave numbers were determined, vibration mode assignments were made and presented in comparison with experimental values in FTIR and Raman spectra. The ionization potential, chemical potential/hardness/softness, electrophilic index, and intramolecular charge transfer information of the hydantoin-based drugs were determined via HOMO-LUMO data. The reactive sites of the hydantoin-based drugs were illuminated with MEP analysis. The molecular orbital energies and occupancies were obtained via NBO analysis. Based on the docking results obtained in this study, phenytoin, mephenytoin, and ethotoin demonstrate a potential anticonvulsant activity by giving binding energy to the GABA-AT receptor of −5.95, −5.55, and −6.68 kcal/mol respectively, similar to isosteviol, carbamazepine, and vigabatrin. MDs and docking simulation results showed that hydantoin-based drug molecules were docked in the binding region of the GABA-AT receptor, especially with ionic interactions. The important findings obtained in this study show that hydantoin-based drug molecules such as phenytoin,

mephenytoin, and ethotoin have nontoxic effects and show drug potential. These results may lead to the development of new anticonvulsant and antiepileptic agents as well as more selective and nontoxic derivatives. Additionally, in the cytotoxicity study, it was determined that phenytoin and mephenytoin had toxic effects on U-87 cells, while ethotoin had proliferative effects on U-87 cells.

Acknowledgments

Authors are thankful to Schrödinger's teams for providing technical support in usage of software of Schrödinger's Small-Molecule Drug Discovery Suite and Desmond Suite. Authors are grateful to TUBITAK 2209A Project for facilitation and support. The FT-IR (transmittance and reflectance) and Raman spectra in this work were recorded at a molecular spectroscopy lab with project number ONAP-2423, which was supported by the Research Funds of Istanbul University.

Data Availability Statement

The data that supports the findings of this study are available in the supplementary material of this article.

References

1. E. Beghi, "The Epidemiology of Epilepsy," *Neuroepidemiology* 54, no. 2 (2020): 185–191.

2. World Health Organization, *Epilepsy: A Public Health Imperative* (Thailand: World Health Organization, 2019).

3. R. D. Thijs, R. Surges, T. J. O'Brien, and J. W. Sander, "Epilepsy in Adults," *Lancet* 393, no. 10172 (2019): 689–701.

4. M. M. Goldenberg, "Overview of Drugs Used for Epilepsy and Seizures: Etiology, Diagnosis, and Treatment," *Pharmacy and Therapeutics* 35, no. 7 (2010): 392.

5. C. L. Harden, "New Antiepileptic Drugs," *Neurology* 44, no. 5 (1994): 787.

6. M. J. McLEAN and R. L. Macdonald, "Sodium Valproate, But Not Ethosuximide, Produces Use-and Voltage-Dependent Limitation of High Frequency Repetitive Firing of Action Potentials of Mouse Central Neurons in Cell Culture," *Journal of Pharmacology and Experimental Therapeutics* 237, no. 3 (1986): 1001–1011.

7. R. V. Wagh, R. V. Antre, R. J. Oswal, and H. M. Nimje, "Anticonvulsant Activity: An Overview," *Journal of Pharmaceutical Science and Bioscientific Research* 1 (2011): 142–147.

8. P. Storici, D. De Biase, F. Bossa, et al., "Structures of γ-Aminobutyric Acid (GABA) Aminotransferase, a Pyridoxal 5′-Phosphate, and [2Fe-2S] Cluster-Containing Enzyme, Complexed With γ-Ethynyl-GABA and With the Antiepilepsy Drug Vigabatrin," *Journal of Biological Chemistry* 279, no. 1 (2004): 363–373.

9. M. Sahu, N. Siddiqui, V. Sharma, and S. Wakode, "5, 6-Dihydropyrimidine-1 (2H)-carbothioamides: Synthesis, in Vitro GABA-AT Screening, Anticonvulsant Activity and Molecular Modelling Study," *Bioorganic Chemistry* 77 (2018): 56–67.

10. R. A. Browning and C. L. Faingold, *Antiepileptic Action of Hydantoins, Drugs for the Control of Epilepsy* (Boca Raton: CRC Press, 2019), 413–424.

11. B. Guldiken, J. Rémi, and S. Noachtar, "Cardiovascular Adverse Effects of Phenytoin," *Journal of Neurology* 263 (2016): 861–870.

12. P. D. Bird, "The Treatment of Autism With Low-Dose Phenytoin: A Case Report," *Journal of Medical Case Reports* 9, no. 1 (2015): 1–5.

13. A. S. Troupin, P. Friel, M. P. Lovely, and A. J. Wilensky, "Clinical Pharmacology of Mephenytoin and Ethotoin," *Annals of Neurology* 6, no. 5 (1979): 410–414.

14. C.-Y. Lee, H.-Y. Lai, A. Chiu, S.-H. Chan, L.-P. Hsiao, and S.-T. Lee, "The Effects of Antiepileptic Drugs on the Growth of Glioblastoma Cell Lines," *Journal of Neuro-Oncology* 127 (2016): 445–453.

15. J. Y. Ryu, K. L. Min, and M. J. Chang, "Effect of Anti-Epileptic Drugs on the Survival of Patients With Glioblastoma Multiforme: A Retrospective, Single-Center Study," *PLoS One* 14, no. 12 (2019): e0225599.

16. M. Stella, G. Baiardi, S. Pasquariello, et al., "Antitumor Potential of Antiepileptic Drugs in Human Glioblastoma: Pharmacological Targets and Clinical Benefits," *Biomedicine* 11, no. 2 (2023): 582.

17. b. N. Sundaraganesan, S. Ilakiamani, H. Saleem, P. M. Wojciechowski, and D. Michalska, "FT-Raman and FT-IR Spectra, Vibrational Assignments and Density Functional Studies of 5-Bromo-2-Nitropyridine," *Spectrochimica Acta Part A: Molecular and Biomolecular Spectroscopy* 61, no. 13–14 (2005): 2995–3001.

18. J. Martin and C. Van Alsenoy, *GAR2PED, a Program to Obtain a Potential Energy Distribution From a Gaussian Archive Record* (Antwerpen, Belgium: University of Antwerp, 2007).

19. H. Gümüş, "2-(2-Hidroksi-5-metoksi-3-nitrobenziliden)-N-metilhi drazin-1-karbotioamid Molekülünün Kuantum Kimyasal Karakterizasyonu," *Muş Alparslan Üniversitesi fen Bilimleri Dergisi* 7, no. 1 (2019): 611–620.

20. S. Kecel-Gunduz, B. Bicak, S. Celik, S. Akyuz, and A. E. Ozel, "Structural and Spectroscopic Investigation on Antioxidant Dipeptide, l-Methionyl-l-Serine: A Combined Experimental and DFT Study," *Journal of Molecular Structure* 1137 (2017): 756–770.

21. Y. Kokcu, S. Kecel-Gunduz, Y. Budama-Kilinc, et al., "Structural Analysis, Molecular Dynamics and Docking Calculations of Skin Protective Tripeptide and Design, Characterization, Cytotoxicity Studies of Its PLGA Nanoparticles," *Journal of Molecular Structure* 1200 (2020): 127046.

22. F. Weinhold and C. R. Landis, *Valency and Bonding: A Natural Bond Orbital Donor-Acceptor Perspective* (Cambridge, UK: Cambridge University Press, 2005).

23. W. Guerrab, H. Lgaz, S. Kansiz, et al., "Synthesis of a Novel Phenytoin Derivative: Crystal Structure, Hirshfeld Surface Analysis and DFT Calculations," *Journal of Molecular Structure* 1205 (2020): 127630.

24. S. Sevvanthi, S. Muthu, and M. Raja, "Quantum Mechanical, Spectroscopic Studies and Molecular Docking Analysis on 5, 5-Diphenylimidazolidine-2,4-Dione," *Journal of Molecular Structure* 1149 (2017): 487–498.

25. H. Lee, E. H. Doud, R. Wu, et al., "Mechanism of Inactivation of γ-Aminobutyric Acid Aminotransferase by (1 S, 3 S)-3-Amino-4-Difluoromethylene-1-Cyclopentanoic Acid (CPP-115)," *Journal of the American Chemical Society* 137, no. 7 (2015): 2628–2640.

26. K. J. Bowers, E. Chow, H. Xu, et al., "Scalable Algorithms for Molecular Dynamics Simulations on Commodity Clusters," in *Proceedings of the 2006 ACM/IEEE Conference on Supercomputing* (Tampa, FL: IEEE, 2006), 84.

27. R. A. Friesner, J. L. Banks, R. B. Murphy, et al., "Glide: A New Approach for Rapid, Accurate Docking and Scoring. 1. Method and Assessment of Docking Accuracy," *Journal of Medicinal Chemistry* 47, no. 7 (2004): 1739–1749.

28. T. A. Halgren, R. B. Murphy, R. A. Friesner, et al., "Glide: A New Approach for Rapid, Accurate Docking and Scoring. 2. Enrichment Factors in Database Screening," *Journal of Medicinal Chemistry* 47, no. 7 (2004): 1750–1759.

29. F. Kiefer, K. Arnold, M. Künzli, L. Bordoli, and T. Schwede, "The SWISS-MODEL Repository and Associated Resources," *Nucleic Acids Research* 37, no. S1 (2009): D387–D392.

30. E. Harder, W. Damm, J. Maple, et al., "OPLS3: A Force Field Providing Broad Coverage of Drug-Like Small Molecules and Proteins," *Journal of Chemical Theory and Computation* 12, no. 1 (2016): 281–296.

31. A. Daina, O. Michielin, and V. Zoete, "SwissADME: A Free Web Tool to Evaluate Pharmacokinetics, Drug-Likeness and Medicinal Chemistry Friendliness of Small Molecules," *Scientific Reports* 7, no. 1 (2017): 42717.

32. S. Lee, S. Park, I. Lee, and K. No, *PreAD-MET Ver. v2. 0* (Seoul, Korea: BMDRC, 2007).

33. D. E. Shaw Research, *Desmond Molecular Dynamics System* (New York, NY: D. E. Shaw Research, 2024).

34. Schrödinger, *Maestro-Desmond Interoperability Tools* (New York, NY: Schrödinger, 2024).

35. P. Mark and L. Nilsson, "Structure and Dynamics of the TIP3P, SPC, and SPC/E Water Models at 298 K," *Journal of Physical Chemistry A* 105, no. 43 (2001): 9954–9960.

36. G. J. Martyna, M. L. Klein, and M. Tuckerman, "Nosé–Hoover Chains: The Canonical Ensemble via Continuous Dynamics," *Journal of Chemical Physics* 97, no. 4 (1992): 2635–2643.

37. G. J. Martyna, D. J. Tobias, and M. L. Klein, "Constant Pressure Molecular Dynamics Algorithms," *Journal of Chemical Physics* 101, no. 5 (1994): 4177–4189.

38. M. J. Frisch, gaussian09, 2009, http://www.gaussian.com/.

39. R. Luchian, E. Vinţeler, C. Chiş, M. Vasilescu, N. Leopold, and V. Chiş, "Molecular Structure of Phenytoin: NMR, UV-Vis and Quantum Chemical Calculations," *Croatica Chemica Acta* 88, no. 4 (2015): 511–522.

40. A. Camerman and N. Camerman, "The Stereochemical Basis of Anticonvulsant Drug Action. I. The Crystal and Molecular Structure of Diphenylhydantoin, a Noncentrosymmetric Structure Solved by Centric Symbolic Addition," *Acta Crystallographica Section B: Structural Crystallography and Crystal Chemistry* 27, no. 11 (1971): 2205–2211.

41. A. Bakalova, H. Varbanov, S. Stanchev, D. Ivanov, and F. Jensen, "DFT Study of the Structure and Spectral Behavior of New pt (II) Complexes With 5-Methyl-5 (4-Pyridyl) Hydantoin," *International Journal of Quantum Chemistry* 109, no. 4 (2009): 826–836.

42. V. Shyni, D. Leenaraj, R. Ittyachan, L. Joseph, and D. Sajan, "Spectroscopic, Density Functional Theoretical Study, Molecular Docking, and In Vitro Studies Based on Anticancer Activity Studies Against A549 Lung Cancer Cell Line of Diphenylhydantoin Adsorbed on AuNPs Surface," *Journal of Molecular Recognition* 34, no. 11 (2021): e2916.

43. P. Marinova, M. Marinov, M. Kazakova, et al., "Study on the Synthesis, Characterization and Bioactivities of 3-Methyl-9′ -Fluorenespiro-5-Hydantoin," *Acta Chimica Slovenica* 63, no. 1 (2016): 26–32.

44. S. Gunasekaran, R. T. Kumar, and S. Ponnusamy, "Vibrational Spectra and Normal Coordinate Analysis of Diazepam, Phenytoin and Phenobarbitone," *Spectrochimica Acta Part A: Molecular and Biomolecular Spectroscopy* 65, no. 5 (2006): 1041–1052.

45. G. O. Ildiz, I. Boz, and O. Unsalan, "FTIR Spectroscopic and Quantum Chemical Studies on Hydantoin," *Optics and Spectroscopy* 112 (2012): 665–670.

46. B. A. Nogueira, G. O. Ildiz, A. M. Tabanez, J. A. Paixão, and R. Fausto, "The Crystal Structure and Raman Spectrum of the Sodium Salt of 5-Acetic Acid Hydantoin," *Journal of Molecular Structure* 1222 (2020): 128897.

47. A. Sharma, V. Gupta, R. Mishra, P. Tandon, S. Maeda, and K.-K. Kunimoto, "Study of Vibrational Spectra and Molecular Structure of Intermolecular Hydrogen Bonded 2-Thiohydantoin Using Density Functional Theory," *Journal of Molecular Structure* 1004, no. 1–3 (2011): 237–247.

48. P. Govindasamy, S. Gunasekaran, and S. Srinivasan, "Molecular Geometry, Conformational, Vibrational Spectroscopic, Molecular Orbital and Mulliken Charge Analysis of 2-Acetoxybenzoic Acid," *Spectrochimica Acta Part A: Molecular and Biomolecular Spectroscopy* 130 (2014): 329–336.

49. J. B. Ott and J. Boerio-Goates, *Chemical Thermodynamics: Advanced Applications* (Bodmin, UK: Academic Press, Elsevier, 2000).

50. D. Sajan, L. Joseph, N. Vijayan, and M. Karabacak, "Natural Bond Orbital Analysis, Electronic Structure, Non-linear Properties and Vibrational Spectral Analysis of L-Histidinium Bromide Monohydrate: A Density Functional Theory," *Spectrochimica Acta Part A: Molecular and Biomolecular Spectroscopy* 81, no. 1 (2011): 85–98.

51. R. S. Mulliken, "A New Electroaffinity Scale:Together With Data on Valence States and on Valence Ionization Potentials and Electron Affinities," *Journal of Chemical Physics* 2, no. 11 (1934): 782–793.

52. M. Govindarajan and M. Karabacak, "Spectroscopic Properties, NLO, HOMO–LUMO and NBO Analysis of 2, 5-Lutidine," *Spectrochimica Acta Part A: Molecular and Biomolecular Spectroscopy* 96 (2012): 421–435.

53. S. B. Prasad, S. Naveen, C. A. Kumar, et al., "Synthesis, Structural Exploration, Spectral and Combinatorial Analysis of Racemic-3-Isobutyl-5-Phenyl-5-(Pyridin-4-Yl) Imida-Zolidine-2, 4-Dione: Comparison Between Experimental and DFT Calculations," *Journal of Molecular Structure* 1167 (2018): 215–226.

54. Y. S. Mary, C. Y. Panicker, M. Sapnakumari, et al., "FT-IR, NBO, HOMO–LUMO, MEP Analysis and Molecular Docking Study of 1-[3-(4-Fluorophenyl)-5-Phenyl-4, 5-Dihydro-1H-Pyrazol-1-Yl] Ethanone," *Spectrochimica Acta Part A: Molecular and Biomolecular Spectroscopy* 136 (2015): 483–493.

55. M. Miar, A. Shiroudi, K. Pourshamsian, A. R. Oliaey, and F. Hatamjafari, "Theoretical Investigations on the HOMO–LUMO Gap and Global Reactivity Descriptor Studies, Natural Bond Orbital, and Nucleus-Independent Chemical Shifts Analyses of 3-Phenylbenzo [d] Thiazole-2 (3 H)-Imine and Its Para-Substituted Derivatives: Solvent and Substituent Effects," *Journal of Chemical Research* 45, no. 1–2 (2021): 147–158.

56. C. T. Zeyrek, Ö. T. Arpacı, M. Arısoy, and F. K. Onurdağ, "Synthesis, Antimicrobial Activity, Density Functional Modelling and Molecular Docking With COVID-19 Main Protease Studies of Benzoxazole Derivative: 2-(p-Chloro-Benzyl)-5-[3-(4-Ethly-1-Piperazynl) Propionamido]-Benzoxazole," *Journal of Molecular Structure* 1237 (2021): 130413.

57. M. Buvaneswari, R. Santhakumari, C. Usha, R. Jayasree, and S. Sagadevan, "Synthesis, Growth, Structural, Spectroscopic, Optical, Thermal, DFT, HOMO–LUMO, MEP, NBO Analysis and Thermodynamic Properties of Vanillin Isonicotinic Hydrazide Single Crystal," *Journal of Molecular Structure* 1243 (2021): 130856.

58. S. Sharma, A. Fatima, F. M. Manhas, et al., "Experimental Spectroscopic, Quantum Chemical, Molecular Docking, and Molecular Dynamic Simulation Studies on Hydantoin (Monomer and Dimer)," *Polycyclic Aromatic Compounds* 43, no. 7 (2023): 6627–6653.

59. S. Hmuda, N. Trišović, J. Rogan, et al., "New Derivatives of Hydantoin as Potential Antiproliferative Agents: Biological and Structural Characterization in Combination With Quantum Chemical Calculations," *Monatshefte für Chemie-Chemical Monthly* 145 (2014): 821–833.

60. G. Serdaroğlu and J. Ortiz, "Ab Initio Calculations on Some Antiepileptic Drugs Such as Phenytoin, Phenbarbital, Ethosuximide and Carbamazepine," *Structural Chemistry* 28 (2017): 957–964.

61. U. Serap and Z. Demircioğlu, "4-Etoksi-3-Metoksibenzaldehit Molekülünün Hesaplamalı Kimya Yöntemiyle Kimyasal Aktivite Tayini," *Karadeniz fen Bilimleri Dergisi* 9, no. 2 (2019): 275–288.

62. B. A. Nogueira, G. Ildiz, J. Canotilho, et al., "5-Methylhydantoin: From Isolated Molecules in a Low-Temperature Argon Matrix to Solid State Polymorphs Characterization," *Journal of Physical Chemistry A* 121, no. 28 (2017): 5267–5279.

63. B. A. Nogueira, G. O. Ildiz, J. Canotilho, M. E. S. Eusebio, and R. Fausto, "Molecular Structure, Infrared Spectra, Photochemistry, and Thermal Properties of 1-Methylhydantoin," *Journal of Physical Chemistry A* 118, no. 31 (2014): 5994–6008.

64. P. Salaria, P. Akshinthala, and R. Kapavarapu, "Identification of Novel C-15 Fluoro Isosteviol Derivatives for GABA-AT Inhibition by In Silico Investigations," *Journal of Molecular Modeling* 29, no. 3 (2023): 76.

65. G. A. Shallangwa, A. Uzairu, and U. Abdulfatai, "Molecular Docking, Design and Pharmacokinetics Study of Some Anti-Epilepsy Compounds," *Modern Applied Science* 15, no. 5 (2021): 1–67.

66. U. Abdulfatai, A. Uzairu, and S. Uba, "Quantitative Structure-Activity Relationship and Molecular Docking Studies of a Series of Quinazolinonyl Analogues as Inhibitors of Gamma Amino Butyric Acid Aminotransferase," *Journal of Advanced Research* 8, no. 1 (2017): 33–43.

67. C. A. Lipinski, F. Lombardo, B. W. Dominy, and P. J. Feeney, "Experimental and Computational Approaches to Estimate Solubility and Permeability in Drug Discovery and Development Settings," *Advanced Drug Delivery Reviews* 64 (2012): 4–17.

68. S. Yamashita, T. Furubayashi, M. Kataoka, T. Sakane, H. Sezaki, and H. Tokuda, "Optimized Conditions for Prediction of Intestinal Drug Permeability Using Caco-2 Cells," *European Journal of Pharmaceutical Sciences* 10, no. 3 (2000): 195–204.

69. T. S. Carpenter, D. A. Kirshner, E. Y. Lau, S. E. Wong, J. P. Nilmeier, and F. C. Lightstone, "A Method to Predict Blood-Brain Barrier Permeability of Drug-Like Compounds Using Molecular Dynamics Simulations," *Biophysical Journal* 107, no. 3 (2014): 630–641.

70. M. Lobell, L. Molnár, and G. M. Keserü, "Recent Advances in the Prediction of Blood–Brain Partitioning From Molecular Structure," *Journal of Pharmaceutical Sciences* 92, no. 2 (2003): 360–370.

71. H. Kubinyi and G. Folkers, *Molecular Drug Properties: Measurement and Prediction* (Darmstadt, Germany: John Wiley & Sons, 2008).

72. T. Lynch and A. Price, "The Effect of Cytochrome P450 Metabolism on Drug Response, Interactions, and Adverse Effects," *American Family Physician* 76, no. 3 (2007): 391–396.

73. J. de Jonge, L. M. Berghauser Pont, S. Idema, et al., "Therapeutic Concentrations of Anti-Epileptic Drugs Do Not Inhibit the Activity of the Oncolytic Adenovirus Delta24-RGD in Malignant Glioma," *Journal of Gene Medicine* 15, no. 3–4 (2013): 134–141.

Supporting Information

Additional supporting information can be found online in the Supporting Information section.